Tip-enhanced Raman Spectroscopy: Principles, Practice, and Applications to Nanospectroscopic Imaging of 2D Materials

Tip-enhanced Raman Spectroscopy: Principles, Practice, and Applications to Nanospectroscopic Imaging of 2D Materials

Feng Shao, and Renato Zenobi*

Department of Chemistry and Applied Biosciences, ETH Zurich, Vladimir-Prelog-Weg 3, CH-8093 Zurich, Switzerland

* zenobi@org.chem.ethz.ch

Abstract

Two-dimensional (2D) materials have been one of the most extensively studied classes of modern materials, due to their astonishing chemical, optical, electronic, and mechanical properties, which are different from their bulk counterparts. The edges, grain boundaries, local strain, chemical bonding, molecular orientation, and the presence of nanodefects in these 2D monolayers (MLs) will strongly affect their properties. Currently, it is still challenging to investigate such atomically thin 2D monolayers with nanoscale spatial resolution, especially in a label-free and non-destructive way. Tip-enhanced Raman spectroscopy (TERS), which combines the merits of both scanning probe microscopy (SPM) and Raman spectroscopy, has become a powerful analytical technique for studying 2D monolayers, because it allows very high-resolution and high-sensitivity local spectroscopic investigation and imaging, and also provides rich chemical information. This review provides a summary of methods to study 2D monolayers and an overview of TERS, followed by an introduction to the current state-of-the-art and theoretical understanding the spatial resolution in TERS experiments. Surface selection rules are also discussed. We then focus on the capabilities and potential of TERS for nanoscale chemical imaging of 2D materials, such as graphene, transition metal dichalcogenides (TMDCs), and 2D polymers. We predict that TERS will become widely accepted and used as a versatile imaging tool for chemical investigation of 2D materials at the nanoscale.

Keywords: Tip-enhanced Raman spectroscopy; Nanoscale chemical imaging; Surface selection rules; Two-dimensional polymers, Monolayers

Introduction

Two-dimensional (2D) monolayers (MLs) are of great importance in both nature and technology due to their unique properties,[1-3] which are different from those of their bulk counterparts. For example, graphene, an atomically thin carbon sheet, is much better than graphite in mechanical strength, electrical and heat conductivity, and exhibits interesting optical and magnetic properties.[4-7] Transition metal dichalcogenides (TMDCs) have tunable electronic properties and variable bandgaps, ranging from insulators (*e.g.,* HfS_2), semiconductors (*e.g.,* MoS_2 and WS_2), semimetals (*e.g.,* WTe_2 and $TiSe_2$), to true metals (*e.g.,* NbS_2 and VSe_2).[8] Exfoliation of these materials into mono- or few-layers can result in additional characteristics owing to confinement effects.[9] A structural analogue of graphene, 2D polymers (2DPs) are covalently linked molecular networks with periodic bonding and repeat units, whose physical and chemical properties depend on the chemistry of their building blocks.[10-13] Compared to graphene, 2DPs possess greater flexibility in composition, porosity, and other physicochemical properties, and can be chemically modified in many different ways,[14-16] contributing to their applications in optoelectronics, catalysis, sensing, and as membranes.[17-19]

Additionally, self-assembled monolayers, a kind of one molecule thick layer of material that binds to a surface in an ordered way, are of vital importance in many applications due to their interfacial properties that influence wettability, adhesion, tribology, and corrosion.[20] Furthermore, biological membranes, with complex, dynamic and temperature-sensitive fluids or gel-like structures, mediate many important cellular processes such as transport of ions or small molecules (hormones, drugs), as well as regulation of cell-cell communication, differentiation and growth.[21,22]

Powerful analytical tools are essential for studying chemical structure, properties, and structure–property relationship of 2D MLs. Spectroscopic investigation of 2D MLs is, however, very challenging due to the following limitations: (i) the spatial resolution of many analytical methods is limited, (ii) the materials is only present in extremely small in amounts (a single molecular layer), and (iii) some 2D MLs are light sensitive. Existing spectroscopic methods like infrared reflection-absorption spectroscopy or enhanced Raman spectroscopy can in principle chemically characterize 2D MLs, but they lack the spatial resolution necessary to determine their structure at the nanoscale. The ideal technique for

investigating 2D MLs should be non-destructive, and capable of gathering molecular information of compounds in a 2D molecular layer with high sensitivity, high spatial resolution, and *in situ*. Methods for nanoscale analysis range from scanning probe microscopy (SPM), electron microscopy (EM), X-ray based spectroscopies, mass spectrometry (MS) based approaches, fluorescence-based and scattering-based optical microscopies, atomic force microscopy (AFM) based optical or force microscopies, to plasmon-enhanced scanning near-field microscopy (SNOM) techniques. All of these techniques have their particular strengths and weaknesses as briefly summarized below in Tab. 1.

Tab. 1 Comparison of analytical techniques for molecular monolayers.

Method	Spatial Resolution	Chemical Sensitivity	Advantages	Disadvantages
AFM,[23,24] STM[14]	< 1 nm	None	Several operating modes (force, conductivity, magnetic, etc.)	No chemical information available
SEM[25,26]	< 1 nm	Only elemental analysis possible (EDX)	Well-established, universal technique, high speed	Usually in UHV (except for environmental SEM), No molecular information available
SAED,[17] LEED[27]	< 1 nm	None	Crystal structure	Damage from high-energy electrons
XPS,[28] NEXAFS[29]	0.5-100 µm	Sub-monolayer	Information on empirical formula, chemical state, electronic state	Limited spatial resolution
SIMS[30]	~50 nm	Sub-monolayer	Specific chemical information (MS)	Only in UHV, destructive
Super-resolving Fluorescence Microscopy[31]	~20 nm	Single molecule (fluorescence probe)	Chemical specificity of fluorescent labels, 3D imaging	Requires labelling by special dyes
AFM-IR,[32] PiFM[33]	10-50 nm	Multiple molecular layers	IR/force spectra, little photodamage	Limited sensitivity or versatility (no measurements in water)
iSCAT[34] *s*-SNOM[35]	10-50 nm	Single molecule	High speed, label-free, dynamics imaging	Limited chemical information
TERS[36]	< 1 nm	Single molecule	Sensitivity, versatility, vibrational fingerprint, orientation dependence	Photodamage effect, tip degradation

***Scanning probe microscopy and electron microscopy*.** Established methods for studying surfaces with nanoscale lateral resolution, such as atomic force microscopy (AFM), scanning tunnelling microscopy (STM), scanning electron microscopy (SEM), and transmission electron microscopy (TEM) based selected area electron diffraction (SAED) and low-energy electron diffraction (LEED) can yield images with high spatial resolution, but typically give very little or no chemical information. There are some exceptions, for example, derivatized AFM tips can be used for specific chemical recognition via force spectroscopy.[37] However, only the shape of nanostructures, the surface topography, the local friction or electric properties can be measured, albeit in many cases with excellent spatial resolution, down to the atomic scale.

X-ray based spectroscopies. Because of different core level energies in various elements, X-ray photoelectron spectroscopy (XPS) and near-edge X-ray absorption fine structure (NEXAFS) spectroscopy can reveal the chemical information about empirical formula, chemical state and electronic state of the elements on a surface from the chemical shift of atomic transitions. Additionally, the composition, conformation and orientation information of thiol SAMs on gold substrates also can also be obtained in principle by XPS and NEXAFS, but, with a micrometer-scale resolution due to the difficulty to focus x-ray.[38,39] Alternatively, XPS images can be possible obtained with a resolution of better than 100 nm using zone-plate technology to focus the x-rays or synchrotron radiation as the x-rays source.[40,41] In these cases, however, rather complicated apparatus and sophisticated conditions are required.

Mass spectrometry. Secondary ion mass spectrometry (SIMS) is the only MS method capable of achieving 50–100 nm spatial resolution, thanks to a tightly focused primary ion beam.[42] SIMS has been successfully employed for chemical imaging of surfaces, including thiol SAMS,[43] DNA monolayers,[44] denatured proteins in adsorbed monolayers,[45] and the nanoscale organization of lipid membranes.[46] However, SIMS is limited to analysis under ultra-high vacuum conditions and is only suitable for detecting elemental or very small molecular species (such as CH, CN) since it is a hard ionization method in its high spatial resolution mode. The static SIMS can only reach a resolution of ≈0.5 μm, comparable to that of optical microscopy.[30,47]

Super-resolving fluorescence microscopies. Brought into the spotlight by the 2014 Nobel Prize in Chemistry, super-resolving fluorescence microscopy methods have been shown to

overcome the diffraction limit and afford nanoscale spatial resolution. These methods rely on experimental modifications and statistical evaluations, including photoactivated localization microscopy (PALM),[48,49] stochastic optical reconstruction microscopy (STORM),[50] saturated pattern excitation microscopy (SPEM),[51] stimulated emission depletion (STED),[52,53] and total internal reflection fluorescence microscopy (TIRFM).[54] Even though PALM can allow localization of fluorescent protein molecules within ≈ 10 nm and STED can reach a spatial resolution of ≈20 nm, a common limitation for all fluorescence-based methodologies is that only the fluorophore can be observed, and unknown compounds in the complex systems go unnoticed.

AFM-based spectroscopies (AFM-IR, PiFM). AFM-IR nanospectroscopy, which combines the spatial resolution of AFM with the chemical analysis capability of IR spectroscopy, relies on detection of the thermal expansion of a sample by illuminating it with the pulse of infrared light and by measuring changes of AFM cantilever deflection. The thermal expansion is proportional to the absorbed light, thus the investigated film is supposed to be thick enough or sensitive enough to detect the thermal expansion.[32] Hence, AFM-IR can be applied for imaging of monolayer graphene with a spatial resolution of ~33 nm,[55] but not for the measurements in liquid due to strong absorption of IR light by water. Additionally, photoinduced force microscopy (PiFM) relies on the mechanical measurement of molecular resonances.[56] Illumination of the sample with laser light induces an oscillating dipole, whose magnitude depends on the local polarizability of the sample. The dipole is mirrored in the metal-coated AFM tip, and the resultant attractive force between the original and mirrored dipoles is measured with the AFM cantilever. Therefore, the optical frequency of the oscillation of molecular polarizability is down-converted to a mechanical frequency of the cantilever's oscillation. By tuning the frequency of the incident laser light, different molecular resonances can be probed, and ultimately a complete vibrational spectrum can be acquired. The method has recently been applied for nanoscale imaging of two-dimensional block copolymer films with a spatial resolution of <10 nm.[33] However, PiFM cannot take advantage of field enhancement and is not sensitive enough to acquire the spectra of single polymer sheets.

Scattering-based optical microscopies. Interferometric scattering microscopy (iSCAT) relies on collecting the interference between a weak reflection light at the sample surface and light scattered by an object in the medium.[57] Temporal resolution and localization

precision can be decoupled from one another in iSCAT imaging.[58] For example, lipid nano-domains as small as 50 nm in droplet interface bilayers can be resolved and dynamics on the millisecond timescale can be established using iSCAT.[34] Since the image contrast in iSCAT stems from differences in refractive index, the method is unable to identify the chemical differences that are responsible for the contrast. Additionally, infrared vibrational scattering scanning near-field microscopy (IR *s*-SNOM) detects light scattered by nanoscale regions under the apex of a metallic AFM tip. The scattered signal of interest arises from the near-field interaction between the tip and sample optical polarization, and can be resonantly enhanced due to the resonance between the vibrational modes in the sample and the incident IR wavelength.[59] IR *s*-SNOM can have access to the structure, coupling, and dynamics information of the sample at molecular length scales,[35] however, it is unable to measure samples in liquid and susceptible to the sample thickness and substrate induced shifts in the position of absorption peaks.[32]

Plasmon-enhanced SNOM. Plasmon-enhanced SNOM techniques can overcome the insufficient sensitivity of the AFM-based methods, and enhance the spectroscopic signal by employing plasmon resonance of the scanning probe. This principle is not only applicable in Raman spectroscopy, but can also be used to enhance fluorescence and photoluminescence.[60] A relevant example is that the individual transmembrane protein in the cell membranes of erythrocytes can be optically resolved by using antenna-based fluorescence imaging in a liquid environment.[61] The distribution of interprotein distances was determined with 50 nm spatial resolution. This approach should also allow one to probe single membrane proteins in live cells with a resolution of 5-10 nm.[61] Furthermore, the photoluminescence quenching center in a MoS_2 monolayer can be determined by tip-enhanced photoluminescence microscopy with a spatial resolution of 20 nm,[62] and internal twin boundaries associated with the expected exciton diffusion length in a monolayer $MoSe_2$ can be resolved with a spatial resolution of around 15 nm.[63]

In this review, we start with an overview of recent methods for nanoscale analysis of 2D monolayers. Next, we will discuss background of TERS, mechanisms of tip enhancement, and technical aspects of TERS, which include optical geometries, SPM feedback, TERS tips, tip lifetime, and TERS imaging. We then introduce the current understanding of the sub-nanometer spatial resolution and surface selection rules of TERS. A focus is then put on the

applications of TERS imaging to 2D materials, including graphene, TMDCs, and 2DPs. Finally, we discuss some challenges and future directions of TERS.

1. Background of TERS

When light encounters molecules, it is possible for the incident photons to scatter inelastically off the molecules and exchange energy, leading to the emission of photons with different frequencies. This effect was first discovered by C.V. Raman and K.S. Krishnan in 1928 in India,[64] and was named Raman scattering. It is a very rare and fast process, with only 10^{-6}-10^{-8} photons of the incident light being inelastically scattered within a picosecond or less.[65] Even though ordinary Raman spectroscopy provides a detailed chemical fingerprint of a sample that can be used for molecular structure analysis and quantification, most molecules have only a very low scattering cross sections in the large of ~10^{-31} - 10^{-28} cm^2 sr^{-1}, leading to very weak Raman signals.[66]

An improvement came with the introduction of surface-enhanced Raman spectroscopy (SERS), which employs metallic nanostructures to cause a very strong local surface plasmon resonance (LSPR) enhancement.[67,68] This local electromagnetic field increases both the absorption as well as the Raman scattering from compounds in a SERS hotspot, which is commonly known as the electromagnetic (EM) mechanism of SERS.[69] Experimentally, the EM mechanism has yielded the enhancement factors on the order of 10^6 ~10^8, which even enables single-molecule detection.[69] Additionally, photo-driven charge transfer (CT) excitations may occur of the adsorbate if the Fermi level of the metal is located between the highest occupied molecular orbital (HOMO) and the lowest unoccupied molecular orbital (LUMO) in energy. This chemical CT mechanism results in an additional enhancement factor ranging from 10^1 to 10^3.[70] SERS has been applied to a wide variety of fields owing to its high sensitivity and because it overcomes the low Raman cross section of many different molecules. However, it still encounters some following drawbacks:[71-74]

1. The optical diffraction limit prevents the SERS signals from a conventional microscope from being spatially resolved beyond ~200 nm.
2. Electromagnetic and chemical enhancements in SERS can be intertwined, and thus, the distinct mechanisms of SERS enhancement are still under discussion.

3. SERS is mainly recorded from rough surfaces of coinage metals, but hardly from smooth or even single crystalline interfaces with only chemical enhancement.
4. The total enhancement depends on the properties of the SERS substrates and the nature of molecules studied.

In order to address these limitations, the theoretical concept of enhanced near-fields was proposed in the 1980s. Around the same time, in 1985, Wessel proposed the idea of TERS, namely, to combine the use of a single metal SERS nanoparticle with a scanning probe microscope (SPM) for obtaining topographic and spectroscopic information simultaneously.[75] He also noted that the nanoparticle can act as an antenna to provide field enhancement for Raman spectroscopy to reach even single molecule detection, while SPM can enable precise control of the particle/tip to reach high spatial resolution.[72] In 2000, the first experimental realization of TERS was demonstrated independently by the groups of Zenobi,[76] Pettiger,[77] Kawata,[78] and Anderson,[79] who used full-metal or metal-coated tips to enhance the Raman signal from surface adsorbed molecules. Upon laser illumination, localized surface plasmons are excited at the tip apex, giving rise to a large enhancement of the electromagnetic field, which greatly increases the Raman scattering of compounds in the vicinity of the tip. In addition to the large enhancement, the TERS effect originates from an extremely small region, typically ≈10 nm.

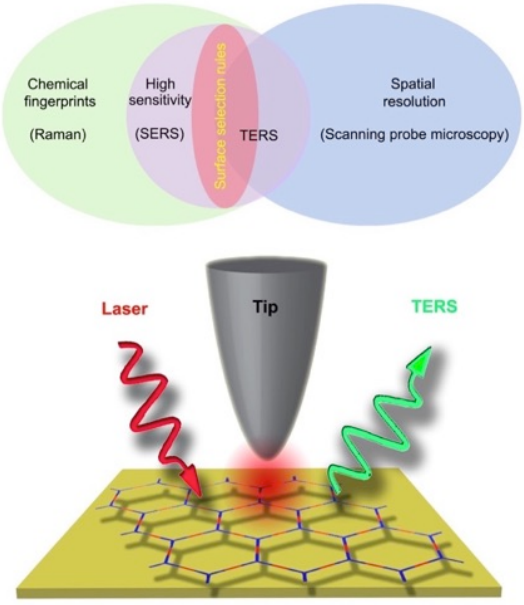

Fig. 1 Venn diagram highlighting the benefits of TERS and basic schematic of the TERS experimental geometry for nanoscale imaging of monolayers.

TERS combines the chemical selectivity of Raman spectroscopy, the sensitivity of SERS, and the lateral resolution of SPM (Fig. 1). It was found that TERS can generally provide an enhancement factor around 10^3-10^6 with a spatial resolution of about 10-80 nm, which clearly breaks the optical diffraction limitation.[71] Compared to confocal Raman spectroscopy, TERS is also affected by surface selection rules, which is similar to the SERS surface selection rules.[80] In general, all Raman-active modes can in principle be observed in a confocal Raman spectrum, where vibrational modes are averaged over all (random) orientations of the molecules present.[81-83] Conversely, when using a metal tip-metal substrate geometry, the TERS spectrum mainly shows the active modes of an adsorbed molecule that follow the selectivity of the Raman response and surface selection rules on metallic substrates. These modes contain significant out-of-plane vibrational components and coincide with the direction of the enhanced plasmonic field.[36,81,84,85] This selectivity also enables TERS to access the orientation/configuration of molecules and monolayers deposited on the conductive, flat surfaces.[86,85]

Despite a much weaker enhancement factor than SERS which is offered by multiple hotspots from laser radiated areas, TERS is still good enough for experimentally measuring samples with a low Raman cross section at the nanoscale, and even reaches single molecule detection sensitivity in favorable cases.[87,88] For instance, experiments carried out under UHV and ultralow temperature, TERS clearly showed the single molecule sensitivity with a sub-nanometer spatial resolution.[73,36] Additionally, by collecting every TERS spectrum at each pixel of a simultaneous scan probe image, TERS imaging opens up a new avenue for surface imaging at the nanoscale, and its general applicability ranges from chemistry, physics, biology to materials science.

2. Tip enhancement

The enhancement mechanisms of TERS are largely the same as those involved in SERS, *i.e.,* EM and CT mechanisms. The EM mechanism also contributes dominantly to the enhancement effect in TERS.[69] It normally contains three different contributions: (i) surface plasmon resonances; (ii) the lightning-rod effect; and (iii) antenna resonances.[89] For a plasmonically active, conductive and sharp nano-tip under laser irradiation, which apex allows for significantly concentrating surface charges, the nano-tip will serve as a

lightning rod leading to strong optical resonances and highly confined local electromagnetic fields. This phenomenon is known as lightning-rod effect.[90,91] The strong electromagnetic field could cause enhanced Raman scattering, resulting in highly intensified and localized Raman signals of molecules under the nano-tip with the confined field far below the diffraction limit. Note that the lightning-rod effect depends on the geometry and conductivity of the tip material and it is independent of the frequency of the incident light.[92] However, if the dimension of the tip is related to an effective incident wavelength, antenna resonances can be formed, similar to the excitation of surface plasmon.[93,94] In this case, these three enhancement mechanisms all contribute, and the highest field enhancement is expected.

When approaching the tip close to (~1-2 nm) a plasmonic substrate (Au, Ag, and Cu) using SPM feedback, even stronger field intensity and confinement can be created due to electromagnetic coupling between the tip and the substrate, which is known as the gap-mode effect, as shown in Fig. 2.[95] Here the nano-cavity between the tip and substrate is spatially confined, and a distinct red shift of the LSPR peak can be observed.[96] Conversely, if there is no coupling between the tip and the substrate, the TERS enhancement could be weaker than that of the coupled case by 2 to 3 orders of magnitude.[97] The enhancement in the nano-cavity shows a d^{-10} dependence (d is the tip-substrate distance), as described previously.[98] Additionally, many other factors also impact the enhancement of the confined field, including the tip material and geometry, incident laser wavelength, focus, polarization, and incident angle.[73]

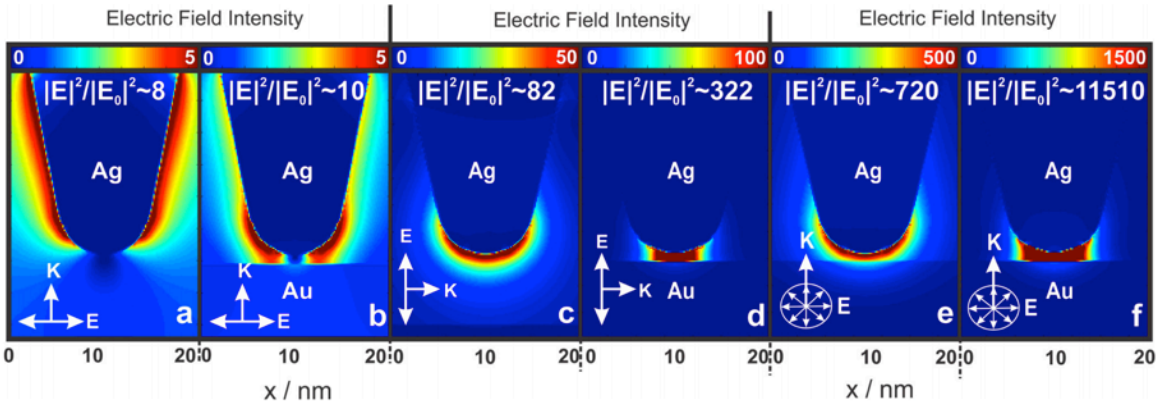

Fig. 2 Electric field distribution at the 10 nm apex of a silver tip illuminated at 532 nm by (a) linearly polarized light along the tip axis, (b) linearly polarized light along the tip axis with 1 nm separation from a gold substrate, (c) linearly polarized light perpendicular to the tip axis, (d) linearly polarized light along the tip axis with 1 nm separation from a silver substrate, (e)

radially polarized light along the tip axis,(f) radially polarized light along the tip axis with 1 nm separation from a gold substrate. (Adapted from [95], Copyright 2013 Optical Society of America)

As shown in Fig. 3, this tip-substrate configuration can be approximated as a system of two metal spheres, one being the tip apex and the other is its image in the substrate.[98] By assuming these two spheres to be equipotential bodies, Xu *et al.* proposed a simple method to estimate the local electric field $\boldsymbol{E_{loc}}$ in the nano-gap as follows:[99,100]

$$\frac{|\boldsymbol{E_{loc}}|}{|\boldsymbol{E_{inc}}|} \approx \frac{\boldsymbol{2R+d}}{\boldsymbol{d}} \tag{1}$$

where $\boldsymbol{R}$ is the radius of curvature of the tip apex and $\boldsymbol{d}$ is the distance between the tip and its image. For a very small $\boldsymbol{d}$, the field enhancement can be approximated as $\boldsymbol{2R/d}$. The full width at half maximum (FWHM) of the field is given by the following equation:

$$\boldsymbol{FWHM = 2\sqrt{Rd}} \tag{2}$$

This result is similar to more accurate calculations.[101] Further simulations based on the finite-difference in the time-domain (FDTD) simulations suggested that $\boldsymbol{E_{loc}}$ is proportional to $\boldsymbol{1/(R+d)^n}$, while the local field is confined in a region with a FWHM is proportional to $\boldsymbol{\sqrt{Rd}}$.[102,103]

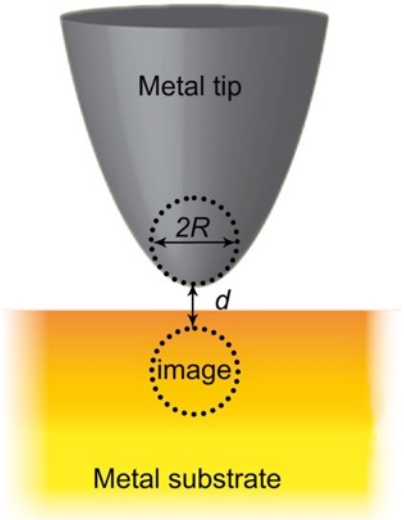

Fig. 3 Scheme of gap-mode TERS with the metal tip-substrate structure approximated as a metal-sphere dimer.

Flat and clean metal substrates can provide a reliable reference surfaces for STM-TERS mapping, which is really necessary for some low dimensional materials, such as CNTs, DNA, graphene, self-assembled monolayers, and 2D polymers. Owing to its physico-chemical properties and its stability, Au is widely used as a substrate in ambient TERS, e.g., template-

stripped Au,[104] flame-annealed Au surfaces,[105] Au nanoplates,[106] semi-transparent Au substrates,[107] and single crystal surfaces.[108,85] Among them, single crystal surfaces are mostly used for investigating molecular orientation by TERS.[81,84,85,108] Furthermore, Stadler *et al.* studied a wide range of rarely used or previously unused substrates (Cu, Ag, Al, Pd, Pt, Ni, Ti, Mo, W, stainless steel, Al_2O_3, SiO_2) in TERS.[97]

3. Technical aspects of TERS

3.1 TERS tips

The tip is the most crucial element in TERS, as it dominates not only the enhancement but also the spatial resolution in TERS imaging. In addition, the activity and stability of the TERS tip determine the quality and reproducibility of TERS measurements. Consequently, fabrication of reliable and highly enhancing TERS tips is essential to the further development and application of TERS. Generally, a full metal or metal coated tip is used to approach the sample surface controlled by an SPM feedback. Several factors are involved in determining the enhancement factor and spatial resolution of the tip, including the material, radius, angle, and morphology of the tip apex.[96] Au and Ag are the most commonly used materials for tip fabrication and for excitation with visible light, because their LSPR wavelength can approximately match with the irradiation laser. In the UV and deep UV spectral regions, Al is a viable choice and Al tip shows a promising enhancement for some special applications.[109,110] In order to obtain high-quality TERS spectra, the lifetime and issues with contamination of the tip also have to be taken into consideration.

AFM-TERS tips

For AFM based TERS, tips are typically fabricated by vacuum evaporation or electrodeposition of the desired metal (Au, Ag, or Al) onto commercially available AFM cantilevers (Si, Si_3N_4). The morphology of the deposited metal films or grains can be affected by the material, evaporation ratio, and whether annealing setup is used.[111-114] Moreover, the plasmonic enhancement of a tip strongly depends on the number of metal grains and on their separations on the tip surface.[94,115]

To tune the LSPR wavelength of an Ag-coated cantilever to be resonant with a green/blue laser, auxiliary layers can be helpful by decreasing the refractive index of the dielectric tip

from Si (n=3.48) to TiO_2 (n=2.75), or SiO_2 (n=1.5) to AlF_3 (n=1.4).[116-118] Another way to tailor the LSPR wavelength of the tip is to increase its length, and such tips can be fabricated by focused ion beam (FIB) milling.[119,120] Additionally, metal-coated AFM tips can also be prepared by pulsed electrodeposition to rationally control the radii of AFM-TERS tips from a few to hundreds of nanometers.[121,122] Furthermore, some specialized AFM-TERS tips are fabricated by chemical bonding nanoparticles to the AFM tip apex,[123-125] electrochemical depositing nanoparticles to the AFM tip apex,[126] or using microfabrication methods.[127-129] In order to take advantage of an etched Au or Ag tip, combining an AFM chip and an etched metal wire was proposed for fabricating full metal AFM-TERS tips.[130]

STM-TERS tips

For STM based TERS, the most common and reproducible method to produce STM-TERS tips is electrochemical (EC) etching of metal wires (Ag and Au). During the etching processes, the metal wire acts as a dissolution anode and the part near the air–liquid interface will be etched to form a neck until it drops off, once it becomes too thin to support the immersed part.[131] Depending on the etching parameters (*e.g.,* voltage, cut-off current, etchant, and temperature), a different radius of curvature can be obtained for the tip apex, which strongly impacts the field enhancement and spatial resolution of the tip. Generally, the radii of curvature range from around 40 nm to 70 nm for etched Ag tips,[132-135] and from 20 nm to 40 nm for etched Au tips.[136-138] Furthermore, the shape, size and geometry of the tip can also be controlled by changing the EC etching parameters.[139] Additionally, some specialized STM-TERS tips are produced by using FIB milling to fabricate gratings on the tip shaft. Owing to the coupling effect of the grating under laser illumination, surface plasmon polaritons (SPP) are excited and propagate to the tip apex for nanoscale excitation.[140,89] For electrochemical applications of STM-TERS at the solid/liquid interfaces, the tip has to be isolated by coating it with a thin layer of polyethylene[141] or Zapon[142,143] to reduce the leakage current.

SFM-TERS tips

For SFM based TERS, almost all kinds of tips can be attached to a tuning fork for shear force feedback, thus this method is similar to the AFM techniques. A distinguishing feature

is that in SFM feedback, the tip, driven by the tuning fork, oscillates horizontally with respect to the sample, and the tip-sample distance is controlled via SFM feedback to around 2-5 nm.[144] Etched Ag or Au tips with proper length are usually glued onto a tuning fork.[86,145-147] In this case, the additional weight of the glued tip and the amount of the glue affect the frequency and quality factor of the tuning fork, i.e., the amount of glue has to be minimized. Furthermore, etched tungsten tips with Au or Ag coating are also used to the SFM-TERS system.[148] Another option is to pull or etch glass fibers and then coat a metal layer or attach nanoparticles to the fiber apex,[149-151] but these procedures appear to be time-consuming, and have low reproducibility.

3.2 Tip lifetime

Despite the ability to provide a stronger field enhancement in the gap-mode TERS, Ag tips are susceptible to chemical and mechanical degradation during the measurements. A possible reason is the high reactivity and low stability of nanorough Ag tips. Therefore, the lifetime of Ag tips is limited to several hours, or at most a few days as reported in the literature.[152-154] Alternatively, Au tips can show a longer lifetime. Therefore, a compromise between enhancement and lifetime has to be found.

On the one hand, some oxygen and sulphur compounds from the atmosphere can react with Ag tips to change their surface plasmon resonance, leading to degradation or inactivation. Two quite noticeable modes at 220-240 cm^{-1} have been assigned to the silver oxides or sulphides on the defect sites of the tips.[155,156] Another significant indicator is a band at around 960-970 cm^{-1} that can appear during TERS mapping, which is related to the silver sulfite (Ag_2SO_3) and silver sulfate (Ag_2SO_4).[157] On the other hand, the Ag tip apex may be worn out or its nanostructure may be changed during scanning, and such mechanical degradation also causes fluctuations in the TERS intensity.[158] For metal-coated AFM tips, the coating layer or particle on the apex can be easily worn out during scanning in contact mode, due to weak adherence between the metal and the underlying tip material.[159] Furthermore, another source of tip degradation may come from heating from laser irradiation and enhanced local plasmon in the confined area.[160-162] If decomposition of organic materials taken place on the tip, two broad bands often appear

after a long time of measurement, centered around 1350 cm^{-1} (D band) and 1580 cm^{-1} (G band), respectively.[163] These peaks can be easily recognized as carbonaceous contamination due to sample degradation within the hotspot nano-cavity.[164,165]

In order to extend the tip lifetime, several strategies have been proposed in the literature, including protective coatings, electrochemical reversal, and environmental control. An additional thin layer, such as SiO_2,[166] Al_2O_3,[154] AlF_3,[167] or a self-assembled monolayer,[167] is helpful to improve the wear resistance and prevent chemical degradation. However, there is a delicate balance between better protection with a thick coating and less enhancement, because a larger tip-sample gap will also decrease the field enhancement of the tip. Moreover, Opilik *et al.* have presented a simple galvanic replacement reaction to recover the activity of corroded silver tips, a recipe that also allows the long-stem storage of Ag tips.[153] Interestingly, Huang *et al.* found that when prepared by the electrodeposition method, the Ag-coated AFM tips exhibit a longer lifetime in the ambient environment (13 days) compared to those prepared by vacuum evaporation (9 hours). This is due to different surface morphologies of the Ag layers and different adhesive strengths between the Ag layers and the tips.[114] The resulting Ag tips are attractive for long time TERS measurements in the ambient environment that require longer times, e.g. imaging experiments.

For the environmental control, Kumar *et al.* have demonstrated that Ag-coated probes stored in a glovebox with sub-ppm oxygen and moisture concentrations have much longer lifetimes (5 months) than those stored in the ambient environment (4-8 hours).[168] Additionally, a large number of studies have demonstrated the benefits of performing TERS in an UHV environment. Under well-controlled conditions, many different molecules and materials can be deposited and studied in an UHV-STM/AFM system, which will greatly improve the tip lifetime, the stability of the tip-sample junction, and minimize contamination of the tips.[73]

3.3 TERS imaging

Since a single point spectrum can only provide a limited amount of information, TERS imaging has become a viable technique to gain information about the local molecular concentration and molecular distribution samples over the entire surface on the nanoscale.

The results can then be statically analyzed. TERS imaging is usually achieved by scanning the surface with SPM feedback while obtaining a TERS spectrum at each pixel.[161]. TERS imaging with the acquisition of a full spectrum at every pixel was used to visualize the distribution of organic molecules and peptide nano-tapes,[104,169] to map the structural inhomogeneity of inorganic crystals,[86] track the strain-induced carbon nanotubes (CNTs)[170], and estimate the conversion ratio in 2D polymer monolayers.[108] Zhang *et al.* reported chemical mapping of single molecules by TERS with an unprecedented, sub-nanometer spatial resolution, which could even resolve the molecule's inner structure.[36]

However, TERS imaging is also affected by several factors, leading to spectral and resolution artifacts:

1. Thermal drift. For TERS under ambient conditions, thermal drift of the TERS setups is unavoidable. Consequently, a compromise between the acquisition time of each pixel and the step size of the imaging has to be found, which may sacrifice the spatial resolution. Thermal drift of a TERS setup can be minimized by continuous scanning until the equilibrium of the system is reached.
2. Thermal diffusion. Due to laser and near-field heating, as well as possibly hot electrons from the substrate, adsorbates may thermally diffuse, leading to fluctuations of molecular orientation, desorption, movements, and even sample decomposition. In this case, some additional signals can occur and peak ratios will fluctuate in the spectra. Moreover, thermal diffusion of sample molecules can also decrease the spatial resolution of TERS imaging. To prevent this problem, one can immobilize molecules on surface, for example, by using a self-assembled monolayer with a thiol-anchor, or by using a low temperature system.
3. Tip degradation. Tip degradation can change the morphology and plasmonic properties of the tip, resulting in the degradation of its enhancement factor and spatial resolution. Generally, the maximum enhancement of the tip and the highest intensity of the signal is obtained at the beginning of recording a TERS map, and then it will get weaker and weaker over time until reaching equilibrium. Based on the sample, materials of the tip and the incident laser power, some experimental parameters have to be optimized. Moreover, protection strategies for the tip can be useful, but at the expense of the enhancement factor and spatial resolution.

Theoretically, quantitative measurements by TERS are possible because the Raman signal intensity is proportional to the probing analytes probed by the hotspot.[163] However, the enhancement in TERS is also subject to variation, due to fluctuations of the laser power, instabilities in the tip-sample distance, and some artifacts mentioned above. Additionally, nano-roughness of the substrate can induce an even higher plasmon enhancement in gap-mode TERS. These temporal changes of the TERS contrast will hamper quantitative measurements by TERS imaging. To address this issue, a straightforward way is to use the intensity ratio of two characteristic peaks from the target compounds[85,108] or mixtures.[171,172,152] By plotting the ratio of the marker peaks, the image contrast can be improved during TERS raster scanning, because signal enhancement is mostly the same within one pixel of an image, even if these pixels may be different from each other. In some cases, a peak ratio is related to the molecular orientation.[108,85] Another approach is to use an internal standard to monitor the variation of the signal enhancement. For example, tip material (*e.g.,* Si)[173] or an additional molecular coating (*e.g.,* a SAM of a thiol)[167] can be used as internal standards for quantitative measurements.

4. Spatial resolution

In optical microscopy, the spatial resolution $\boldsymbol{\Delta x}$ can simply be understood as the minimum distance between two objects that can be unambiguously distinguished. In the 19th century, Abbe and Rayleigh derived the criterion for the spatial resolution of an optical system as follows,[174,175]

$$\boldsymbol{\Delta x} = \frac{\mathbf{0.61}\boldsymbol{\lambda}}{\boldsymbol{NA}} \tag{3}$$

where $\boldsymbol{\lambda}$ is the wavelength of the light, and $\boldsymbol{NA}$ is the numerical aperture of the optical system, which depends on the refractive index of the medium. The value of $\boldsymbol{\Delta x}$ is often approximated as half the irradiation wavelength, thus resulting in a diffraction-limited optical resolution of 200-300 nm when using visible light. In general, this value is the best spatial resolution achieved by confocal Raman spectroscopy and SERS systems.

In TERS, the diffraction limit does not play a role because the Raman signals are dominated by the molecules in the nano-cavity where the electromagnetic field is highly enhanced and confined. Generally, a spatial resolution of ~10-80 nm has been reported for TERS, which is in accordance with the diameter of a typical SPM tip apex.[100] In such a

context, the spatial resolution of TERS would simply be limited by the geometry of the tip apex. Recently, however, several experimental results have shown unprecedented TERS spatial resolution down to the sub-nanometer regime. Almost all of these results were obtained in ultrahigh vacuum and low temperature systems operating with gap-mode STM-TERS.[36,81,170,176-179] This surprisingly good spatial resolution is considerably smaller than the tip apex diameter, so that it cannot be explained by the size, shape, and material of the nano-tip at the apex.

There are several experimental prerequisites for reaching sub-nanometer resolution in TERS. (i) Analytes. TERS experiments with sub-nanometer resolution have almost exclusively been done with resonant porphyrin molecules[36,81,177-179] or very strong Raman scatterers like CNTs[170]. One exception is a study of (non-resonant) DNA bases in a hydrogen bonded network [176], in which sub-nanometer resolution (~0.9 nm) was demonstrated in an ultrahigh vacuum (~1×10^{-10} Torr) and low temperature (80K) system. However, it was impossible to resolve isolated single adenine and thymine molecules at room temperature or even at 80 K in TERS experiments, probably due to the weak interaction between the DNA bases and the Ag(111) surface.[176] (ii) Tip-substrate geometry. In all of these studies, the combinations Ag tip – Ag substrate[81,176], Ag tip – Au substrate,[178,179] or Ag tip – Cu substrate [177] have been used. It therefore appears that gap-mode STM-TERS is required for reaching the single-molecule sensitivity and sub-nanometer spatial resolution. Note that a better spatial resolution automatically implies a smaller number of molecules (down to single molecules) under the TERS tip. (iii) Exciting laser lines. To be resonant with the tip-substrate geometry, 532 nm (Ag tip – Ag substrate geometry),[81,176] 561 nm (Ag tip – Cu substrate geometry),[177] and 634 nm (Ag tip – Au substrate geometry)[178,179] lasers have been used in sub-nanometer spatial resolution TERS, for establishing a strong plasmon resonance. In other words, a certain size of the tip and a proper gap-mode geometry are also required for resonance with the irradiating laser.

To achieve sub-nanometer resolution at ambient conditions is another general pursuit in TERS community, which has been reported on single-stranded DNA sequences [180] and individual amyloid fibrils [181] with AFM-TERS. In light of the discussion above, these results are surprising: these biological macromolecules are generally weak Raman scatterers [182] and basically hard to detect with AFM-TERS because of its lower enhancement [95, 183] compared to, for example, gap-mode STM TERS. For this reason and because of thermal

drift, imaging of such samples has not been possible with AFM-TERS at room temperature. Also, degradation of molecules can occur at room temperature under the tip and lead to spurious peaks [184]. A very interesting theoretical suggestion to explain these findings is that a single atom on spherical plasmonic particles (Ag, Au) acts as a ''super tip'' in gap-mode TERS, and drastically increases the lateral resolution to the sub-nanometer level within the tip-substrate cavity.[185] Such single atomic cavities are dynamic at room temperature,[186] i.e., it is unclear whether such a sub-nanometer, single atom cavity "super tip" is indeed stable at ambient conditions. Consequently, much more work will be needed in this direction.

Until now, the physical mechanisms underlying the sub-nanometer spatial resolution TERS still is not understood. This has of course attracted the theoretical community during the past years. For instance, by the finite element method (FEM), Meng *et al.* found that the confined electric field and its gradients contribute to the resolution in the gap-mode, owning to the field's tighter spatial confinement.[187] They also report a higher sensitivity to infrared (IR)-active modes of molecules under the tip. Duan *et al.* reported that the increase in the nonlinear contribution to the total Raman intensity can further improve the lateral resolution of a Raman/TERS image based on calculations using a higher-order confinement from stimulated Raman scattering.[188] Shortly after, they proposed a general quantum chemical approach to describe resonant and non-resonant Raman scattering in the localized plasmonic field. Under an inhomogeneous field, their calculations demonstrated that an individual vibrational mode of the molecule can be distinguished only in resonant Raman images, and that nonlinear effects can further improve the resolution of the images.[189]

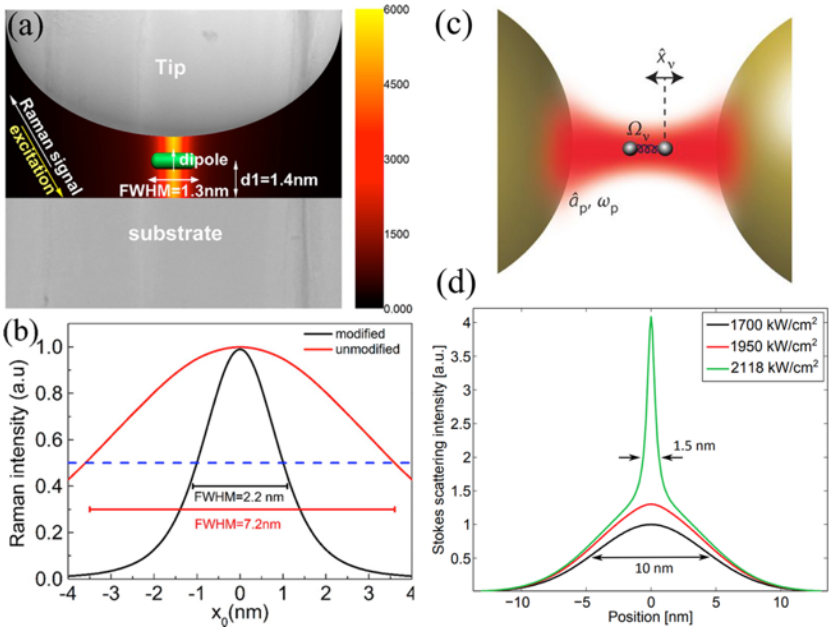

Fig. 4 (a) Scheme of the coupled molecular dipole-local field system involving molecular self-interaction via multiple elastic scattering. (b) Comparison of the TERS lateral resolution predicted by the theory with (black) and without (red) molecular self-interaction. (Reprinted with permission from [190], copyright 2015 American Chemical Society) (c) Schematic mapping of a coupled molecule-plasmon system in a normal coordinate $\hat{x}$ between a mechanical oscillation Ω_v and a cavity of frequency ω_p with occupation $\hat{a}_{p'}$. (d) Computed Stokes scattering intensity as a function of lateral position assuming a point-source scatterer located at the origin. (Reprinted with permission from [191], copyright 2016 Macmillan Publishers Ltd.)

Due to multiple elastic scattering of light by a molecule in the nanogap (Fig. 4a), Zhang *et al.* proposed that the near-field self-interaction of this molecule with the plasmonic nanogap in both the Raman excitation and radiation processes can lead to sub-nanometer spatial resolution in TERS mapping (Fig. 4b).[190] In order to consider the coupling between molecular vibrations and plasons, Roelli *et al.* introduced a canonical model of cavity optomechanics that accounts for the dynamic nature of the plasmon–molecule interaction.[191] Their theory depends on a coherent coupling between a mechanical oscillator (the molecular vibrations) and an electromagnetic cavity mode (the localized plasmon), which can be applied to both SERS and TERS (Fig. 4c). Interestingly, their model also predicts a large nonlinear Raman response when the incident laser intensity approaches the threshold of parametric instability, leading to a sharp increase in spatial resolution (Fig. 4d). That may be used for interpreting the sub-nanometer spatial resolution in TERS.

Furthermore, atomic features on the tip and chemical enhancement effects of molecules also have been considered for TERS with sub-nanometer spatial resolution.[185,192] To provide a consistent treatment of a molecule in the plasmonic near field, Liu et al. reported a hybrid quantum mechanical method that combined atomistic electrodynamics with time-dependent density functional theory, and thus is well-suited for describing single-molecule TERS imaging with atomic resolution (Fig. 7).[193] Using water as a simple model system (Fig. 7b-7d), they demonstrate that TERS images are extremely sensitive to the near field in the junction. in addition, achieving atomic resolution required the near field to be confined within a few Ångstroms in diameter. The best resolution can be obtained when the focal plane (the field maximum height relative to the molecule plane) overlaps with the molecular plane.

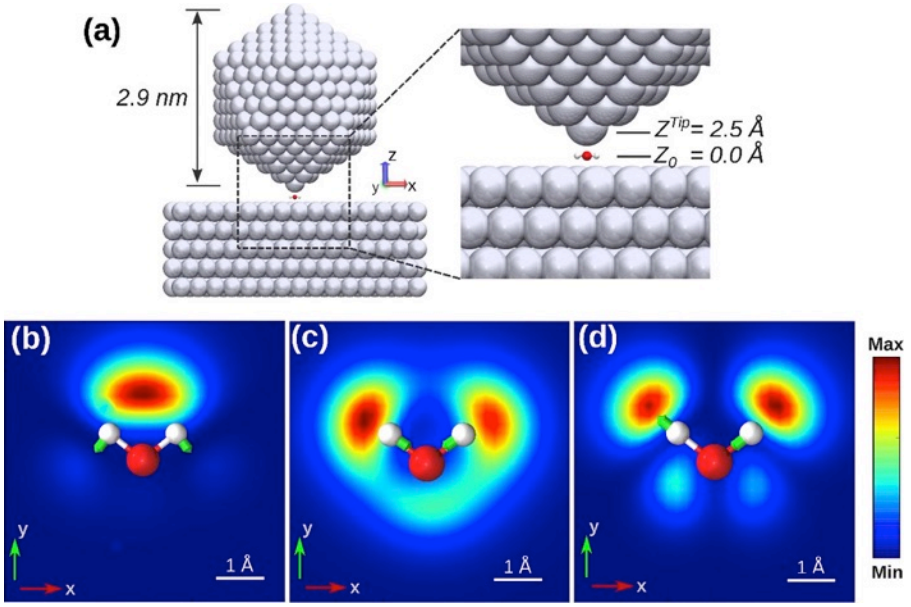

Fig. 5 (a) Scheme of an Ag tip-substrate nanojuction in TERS. Simulated TERS images of different vibrational modes of a single water molecule: (b) bending mode at 1600 cm^{-1}; (c) symmetric stretching mode at 3676 cm^{-1}; (d) antisymmetric stretching mode at 3776 cm^{-1}. (Adapted from [193], copyright 2017 American Chemical Society)

Since many factors, e.g., enhancement processes, near-field effects, changes of selection rules, and system coupling, are involved in determining TERS spectra, theoretical explanations for sub-nanometer spatial resolution observed in TERS are extremely complex and are still ongoing. In practice, to achieve sub-nanometer spatial resolution, several factors need to be well controlled in TERS experiments, such as thermal diffusion of the molecule, thermal drift of the setup, step size of the TERS mapping, incident laser polarization and angle, and nano-features on the substrate, which can all influence the

lateral resolution, and even cause experimental errors or artefacts.[100] In terms of system stability and tip quality, UHV and low temperature systems can generally deliver sub-nanometer spatial resolution in TERS. Additionally, to provide a larger amount of statistical data, TERS imaging is helpful to unambiguously prove a certain spatial resolution. Last but not least, it is important to pay attention to the problem of molecular decomposition under the tip at room temperature, which may lead to spectral changes that could be erroneously interpreted as appearance of new/different molecules.

5. Surface selection rules

In IR spectroscopy, vibrational modes of molecules, when adsorbed on flat, metallic substrates, are subject to surface selection rules:[194,195] the transision dipole moment $\boldsymbol{\mu}$, induces an image dipole inside the metallic substrate. When perpendicular to the surface, the dipole will be doubled, whereas the parallel components will be canceled by the image dipole (Fig. 8). In other words, for adsorbates on the surface, only those vibrational modes which induce a transition dipole perpendicular to the surface are IR active and give rise to an observable absorption band.[196]

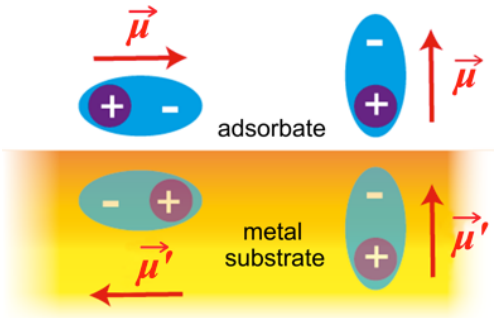

Fig. 6 Schematic illustration of the operation of an adsorbate dipole selection rule on a metallic substrate. The image dipole within the substrate compensates the effect of the dipole for parallel orientation, but enhances the effect of the dipole with a perpendicular orientation.

For Raman spectroscopy, it is the anisotropic polarizability tensor as defined as a 3×3 matrix that must be considered,[197,198]

$$\boldsymbol{\alpha} = \begin{pmatrix} \boldsymbol{\alpha_{xx}} & \boldsymbol{\alpha_{xy}} & \boldsymbol{\alpha_{xz}} \\ \boldsymbol{\alpha_{yx}} & \boldsymbol{\alpha_{yy}} & \boldsymbol{\alpha_{yz}} \\ \boldsymbol{\alpha_{zx}} & \boldsymbol{\alpha_{zy}} & \boldsymbol{\alpha_{zz}} \end{pmatrix} \quad (4)$$

Here, x, y and z are rectangular coordinate axes, which are fixed on the molecule but otherwise chosen arbitrarily. All $\boldsymbol{\alpha}_{ij}$ are the components of the polarizability tensor $\boldsymbol{\alpha}$. For

example, $\boldsymbol{\alpha}_{yx}$ means that an electric-field applied in the x-direction will polarize the material in the y-direction.[199] The polarizability tensor $\boldsymbol{\alpha}$ can be described by a real, symmetric matrix, with all $\boldsymbol{\alpha}_{ij} = \boldsymbol{\alpha}_{ji}$. Thus, it has three diagonal components and three off-diagonal components, and only six tensor components need to be determined. This matrix is only necessarily symmetric in the case of non-resonant Raman scattering. The Raman tensor $\boldsymbol{\alpha}'$ is obtained as the first derivative of the polarizability tensor $\boldsymbol{\alpha}$ with respect to the vibrational normal coordinate.[200]

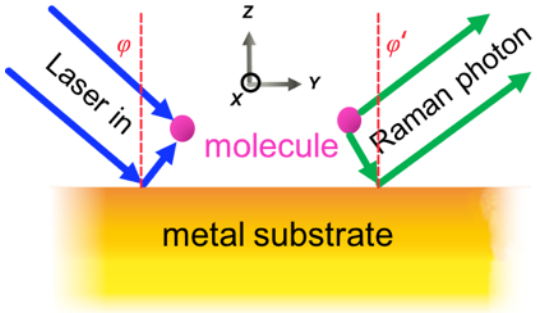

Fig. 7 Scheme of the reflection enhancement for the incident (left) and scattered (right) processes. The **XYZ** axes indicate the coordinates of the molecule.

Since incident light is reflected off metals, a molecule will be exposed to a different electric field when it adsorbed on a flat, metal surface. For a molecule placed right at the surface, the scattered radiation will consist of the coherent superposition of both the incident and scattered waves (Fig. 7), and one gets the effective scattering intensity of the molecule as follows:[195,74]

$$I_{sca}^{eff} \propto \left|\boldsymbol{\alpha}'_{zz}\left(1+r_p\right)\left(1+r'_p\right)\right|^2 \sin^2\varphi \sin^2\varphi' \qquad (5)$$

where r_p and r'_p are the reflected and scattered Fresnel coefficients at the interface for p-polarized (parallel to the plane of incidence) light, respectively. φ and φ' are the angles of incidence and scattering, respectively. $\boldsymbol{\alpha}'_{zz}$ is the Raman tensor of the involved molecular vibration in the Z direction.

Note that the effective Raman component which survives on the surface depends on the z component of the Raman tensor ($\boldsymbol{\alpha}'_{zz}$), which is not usually measured in ordinary Raman spectroscopy.[195] This can be regarded as a surface selection rules, which relates directly to the orientation of the molecule. Importantly, this is different from SERS: because sample molecules are localized in random SERS hot spots with a variety of orientations/configurations compared to the enhanced field direction, the local field in

normal SERS is usually treated as orientation-independent. Therefore, for the conventional description of SERS, the signals are averaged. However, for a single molecule or monolayer in the nano-cavity between a TERS tip and a metal substrate, the molecular orientation/configuration and local field direction can dramatically impact the final Raman/TERS signal.[81] Furthermore, similar surface selection rules in SERS can also be observed when there are homogeneously distributed SERS hot spots.

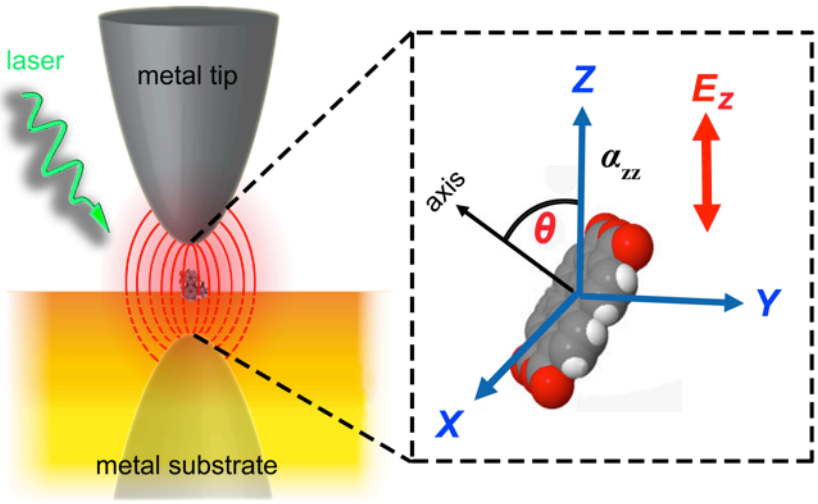

Fig. 8 Schematic of the gap-mode TERS in the side-illumination configuration. The incident far-field radiation induces a strong and confined plasmon field within the gap nano-cavity. The dashed box indicates the frame of reference of the molecule and the coordinates of the plasmonic field, in which is mainly confined and enhanced in the z direction. The black axis arrow (labelled "axis") indicates the defined normal direction of the molecule.

According to FDTD calculations (Fig.2), a tip illuminated by a XY polarized beam, will exhibit an overall electric field intensity of almost zero below its apex in the gap-mode configuration. Consequently, an enhancement matrix, $\boldsymbol{G}$, can be introduced in the gap-mode TERS as follows:[81]

$$G = \begin{pmatrix} \boldsymbol{G_{xx}} & \mathbf{0} & \mathbf{0} \\ \mathbf{0} & \boldsymbol{G_{yy}} & \mathbf{0} \\ \mathbf{0} & \mathbf{0} & \boldsymbol{G_{zz}} \end{pmatrix} \approx \begin{pmatrix} \mathbf{0} & \mathbf{0} & \mathbf{0} \\ \mathbf{0} & \mathbf{0} & \mathbf{0} \\ \mathbf{0} & \mathbf{0} & \boldsymbol{G_{zz}} \end{pmatrix} \tag{6}$$

For a gap-mode TERS setup with a selected polarization and incident angle of the incident light, the local field is thus mostly confined and enhanced in z direction (Fig. 8). Consequently, enhancement components parallel to the surface can be ignored, and the effective intensity of TERS signals can be approximately expressed as below:[81]

$$I_{TERS}^{eff} \propto |G'(\omega_{inc}) \cdot \alpha'_{zz} \cdot G(\omega_{sca})|^2 \quad (7)$$

where $G'(\omega_{inc})$ is the enhancement matrix from the incident light (ω_{inc}), and $G(\omega sca)$is the enhancement matrix from the scattered light (ω_{sca}).

If the molecular normal direction is parallel to the direction of the enhanced field, (angle $\theta \approx 0$, see Fig. 8), the TERS signals is only associated with the α'_{zz} component. As a corollary, when a molecule is tilted on the surface, other compounds of the polarizability tensor will contribute to a new efficient component ($\widehat{\alpha'_{zz}}$). As a result, some modes will disappear and extra modes will appear when the molecule is tilted on the surface, and the corresponding signal intensity of each mode will vary with the tilt angle.[81]

It is worth noting that the abovementioned assumptions are based on a simplified, free space Raman tensor model without considering intermolecular and molecule-substrate interactions. In particular, when a molecule is strongly chemisorbed on the surface, its geometry and configuration may be changed significantly due to the interaction with the surface, and thus leading to breaking of the system symmetry. In this case, some Raman silent modes may become Raman active. Additionally, the light–plasmon coupling in TERS can also modify the classical Raman selection rules, caused by photon tunneling through perturbation of the evanescent field.[201]

6. Applications: TERS imaging of 2D materials

6.1. Graphene

After the first exfoliation of monolayer graphene from graphite in 2004,[202] graphene has stimulated tremendous research interests about 2D materials. Since the disorder-induced D band around 1350 cm^{-1} is a defect related Raman mode, Raman spectroscopy is particularly useful for characterizing defects in graphene.[203,204] However, the D band signal from a single point defect (with a radius of a few nanometers) cannot be detected with confocal Raman spectroscopy. Consequently, to characterize local defects within graphene has become one of most prominent applications for TERS imaging.[205] Generally, local defects can strongly affect the mechanical strength,[6,206] cause poor fracture characteristics,[207] and degrade the electronic performance of graphene.[208] However, it

can also induce magnetism in graphene,[209] increase grain boundary strength,[210] and enhance the conductivity of graphene nanoribbons.[211]

Stadler *et al.* showed the first TERS image of monolayer graphene using a top-illumination STM-TERS setup in 2011 (Fig. 9a-11d).[212] On the monolayer graphene produced by chemical vapor deposition (CVD) on a copper foil, their TERS images were able to identify pristine, defective, contaminated area, and hydrogen-terminated areas with a spatial resolution of <12 nm due to different spectroscopic signatures. Based on the D band intensity, single point defects created by ion bombardment [213] or intrinsic line defects [214] within graphene have also been visualized by AFM-TERS mapping with bottom-illumination, with a spatial resolution of ~20 nm. Recently, Li *et al.* found that an Ag-coated AFM tip can induce atomic deformations when the tip attached to a graphene surface, and that these defects are reversible.[215]

Graphene edges and grain boundaries can be treated as special types of defects, because they break the entire symmetry of the graphene lattice.[205] Su *et al.* used TERS imaging to locate the edges of monolayer graphene, and to improve measurement accuracy of the phase-breaking length ($L_\sigma \approx 4.2\ \mathrm{nm}$) based on the edges' D band intensity.[216] Shortly after, they reported that the D band is highly localized in graphene[217], as expected from confocal Raman measurements.[218] As shown in Fig. 9e-11g, the TERS images of the D (green), G (blue), and G' (red) bands correlate with the topographic image of a graphene sample,[214] and the corresponding spectra demonstrate the ability of TERS tips to enhance weak D and G band signals from localized defects.[214] For a twisted bilayer in CVD grown large-area graphene, Park *et al.* reported high-resolution ($\approx 18\ \mathrm{nm}$) multispectral TERS images to provide a better understanding of the lattice and electronic structure, as well as elastic and phonon scattering properties of grain boundaries.[219]

Structural deformations, *e.g.,* local strain, can change the interatomic distance, redistribute the electronic charge, or even open the band gap in graphene.[204] However, the two most commonly studied types of strain in graphene, uniaxial and biaxial, cannot be characterized by far-field Raman spectroscopy.[205] Snitka *et al.* used tapping mode AFM-TERS with special tips fabricated by flattening Au microwires to investigate the effect of tip pressure on graphene.[220] They observed that the G mode of graphene is shifted and the Raman intensity of the 2D band fluctuates when local strain is induced by the gold tip. Furthermore, Beams *et al.* demonstrated that TERS can be used to map out locally static

strain fields in single layer graphene at the nanoscale, where a 5 nm particle underneath the graphene exerted a local radial strain. These are inaccessible using force-displacement techniques.[221]

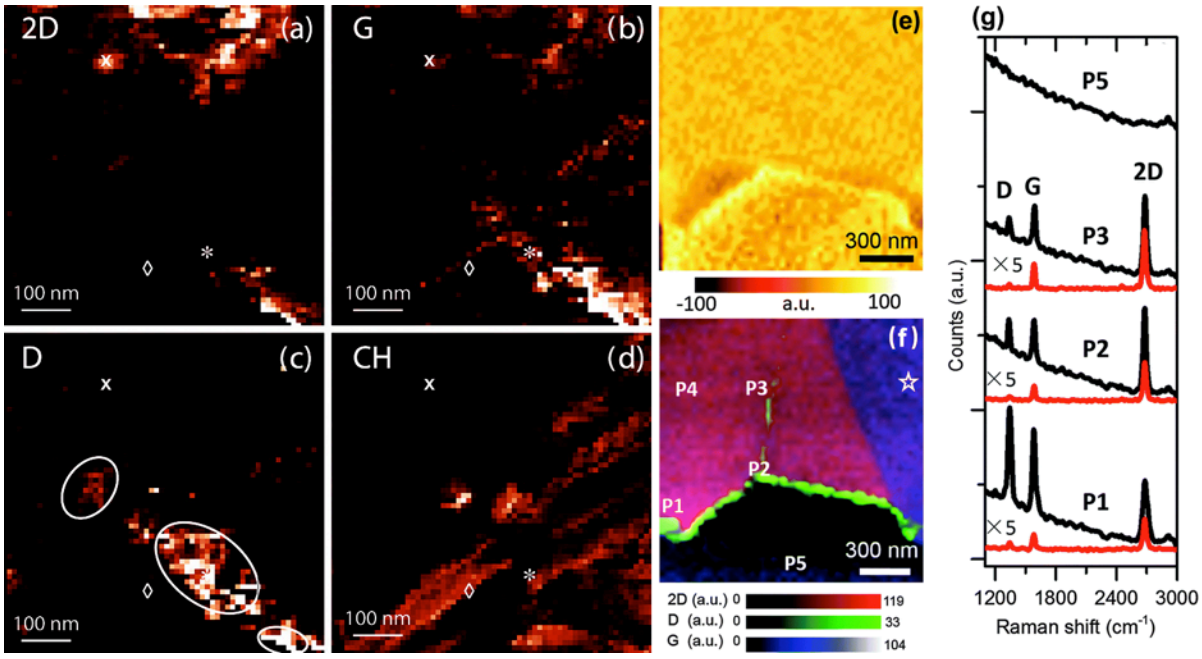

Fig. 9 Raman image of graphene on Cu. Background and enhancement corrected band intensity of the (a) 2D-band at 2634cm^{-1}, (b) G band at 1580cm^{-1}, (c) D band at 1350cm^{-1}, and (d) CH stretching mode at 2800-3000cm^{-1}. The maps show clear localization of graphene defects (c) and the complementary behaviour of the 2D (a) and CH bands (d). (Adapted from [212], copyright 2011 American Chemical Society). (e) Topographic image of a graphene sample. (f) TERS image of the graphene sample with the D (green), G (blue), and G' (red) overlaid. (g) Spectra with (black) and without (red) the tip at the locations labelled in (f). (Adapted from[214], copyright 2016 The Royal Society of Chemistry)

6.2. Transition metal dichalcogenides

Many TMDCs materials, such as $NbSe_2$, MoS_2, $MoSe_2$, WS_2, WSe_2 and TaS_2, are structurally similar but have an array of electronic properties, ranging from semiconducting to metallic, which give rise to some unusual properties and phenomena (*e.g.,* lattice-symmetry-induced valley Hall effect, valley polarization, and superconductivity).[222] Local structural heterogeneities, including doping, defects, and strain in TMDCs can also affect their intrinsic quantum properties,[223] which were investigated by tip-enhanced photoluminescence (TEPL) mapping at the nanoscale.[224,225] However, it is still challenging to understand the relation between the PL intensity, line shape, spectral position and its structural heterogeneities.[63] As shown in Fig. 10, Park *et al.* reported a hybrid nano-optomechanical approach combining TERS, TEPL and atomic force local strain control to study the associated

effects on the excitonic properties in monolayer WSe_2 with a spatial resolution of ~15 nm.[63] Through controlled tip–sample force interaction with a SFM feedback, the bandgap can be tuned *via* local nanoscale strain engineering (0–1%, Fig.12c). Specifically, the combined results enable one to separate the effect of strain from controlling the photoluminescence modification at edges, nucleation sites, and twin boundaries, suggesting that the defects and stoichiometry are the primary factors that affect the photoluminescence at the structural heterogeneities.

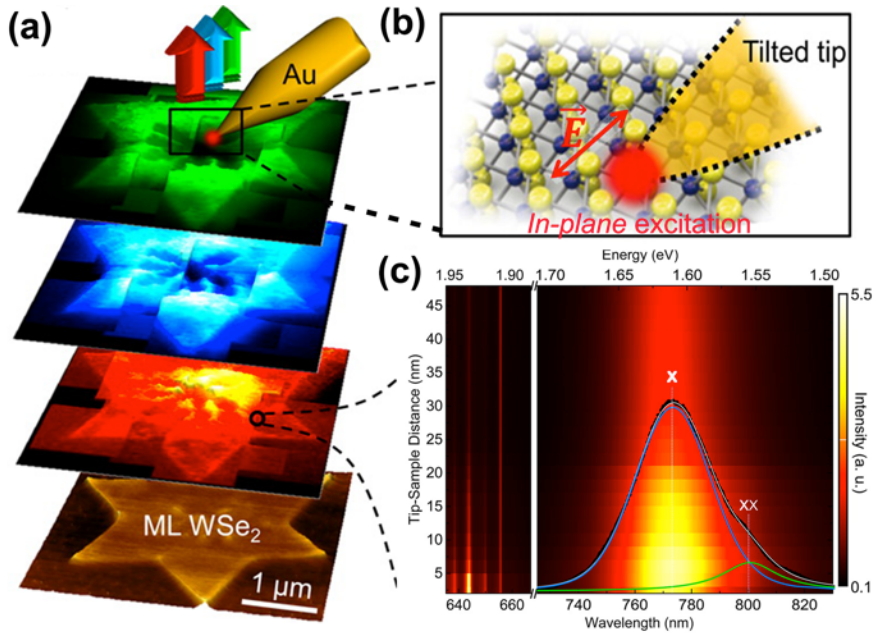

Fig. 10 (a) Schematic of multimodal TEPL/TERS imaging of monolayer WSe_2 with (b) top illumination of a shear-force atomic force microscope tip. (c) Tip–sample distance dependence of TEPL and TERS of monolayer WSe_2. Measured TEPL spectrum (black) at 6 mm distance with Voigt profile fit (gray) decomposed into exciton (blue, X), and possibly biexciton (green, XX) emission. (Reprinted with permission from [63], copyright 2015 American Chemical Society).

To induce highly localized strain, Rahaman *et al.* mechanically deposited tri-layer MoS_2 on a hexagonal periodic array of gold nanotriangles. Through AFM-TERS imaging with a side-illumination configuration, they observed that the frequency of the E_{2g} mode of the ultrathin MoS_2 with local strain shifted by around 4.2 cm^{-1}, corresponding to 1.4% of biaxial strain induced in the MoS_2/Au heterostructure.[226] In analogy, apart from local strain, Milekhin *et al.* reported an unprecedented giant enhancement (by a factor of 5.6×10^8) and an excellent spatial resolution of 2.3 nm from a monolayer MoS_2 flake stamped onto Au nanocluster arrays, using gap-mode AFM-TERS (Fig. 11).[227] Specifically, due to strong hot

electron doping through the plasmonic coupling between MoS_2 and Au nanoclusters, their TERS spectra indicated that there is a structural change of MoS_2 from the 2H to the 1T phase during TERS imaging.[227] These examples illustrate that TERS can be used to investigate local structural heterogeneities in such inorganic 2D materials at the nanoscale, which is of great importance for potential device applications.

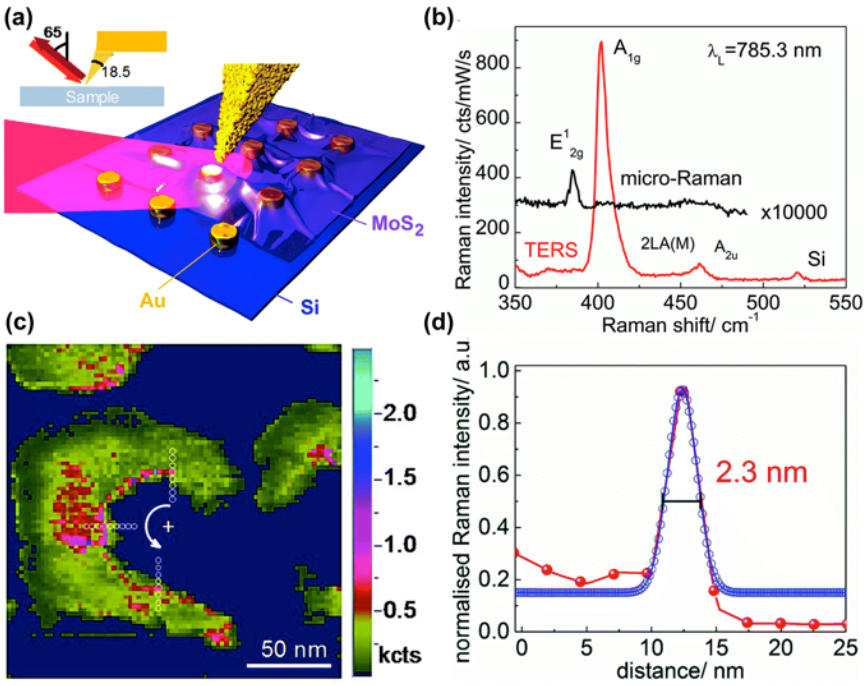

Fig. 11 (a) Scheme of the TERS experiment on a MoS_2 monolayer stamped onto Au nanocluster arrays. (b) A representative TERS spectrum of a MoS_2 monolayer on an Au nanocluster array in comparison with the spectrum excited by 785.3 nm light. (c) A high-resolution TERS image of the A_1g mode of MoS_2 on Au nanoclusters. The false colors represent the intensities of the A_1g mode and form a semi-ring on Au nanoclusters. To determine the spatial resolution, several intensity profiles across the border line of the semi-ring were taken as shown by white open circles. (d) Gaussian fit of the intensity profile. The spatial resolution of the TERS image is equal to the full width at half maximum (FWHM) of the fit (2.3 nm). (Reprinted with permission from [227], copyright 2018 Royal Society of Chemistry)

6.3. 2D polymers

In recent years, 2DPs have emerged as a new type of 2D material with customized and tunable properties.[10-12] 2DPs are considered structural analogues of graphene. The existing tools to synthesize 2DPs primarily rely on the single-crystal and the air/water interface methods. The single-crystal approaches are mostly used for 2DPs prepared by photo-chemically induced [4+4]-cycloadditions of anthracene-based monomers, or thermally initiated C-C cross-coupling of tetrabromopolyaromatic monomers,[15,228-231]

followed by exfoliating into single sheets. The air/water interface approach can produce large-area 2D covalent MLs ranging from tens of micrometers to wafer size.[12,17] These 2D covalent MLs are mainly obtained from photo-polymerization under ultraviolet irradiation of amphiphilic anthracene-derivatives,[14,232] co-ordination chemistry with metal ions,[233-235] or dynamic imine chemistry with a Schiff base,[12,17] using a Langmuir-Blodgett (LB) trough. To characterize 2DPs, TERS has established itself as a promising method, because it allows very high-resolution, high-sensitivity, local spectroscopic investigation and imaging, and provides rich chemical information in a label-free fashion.

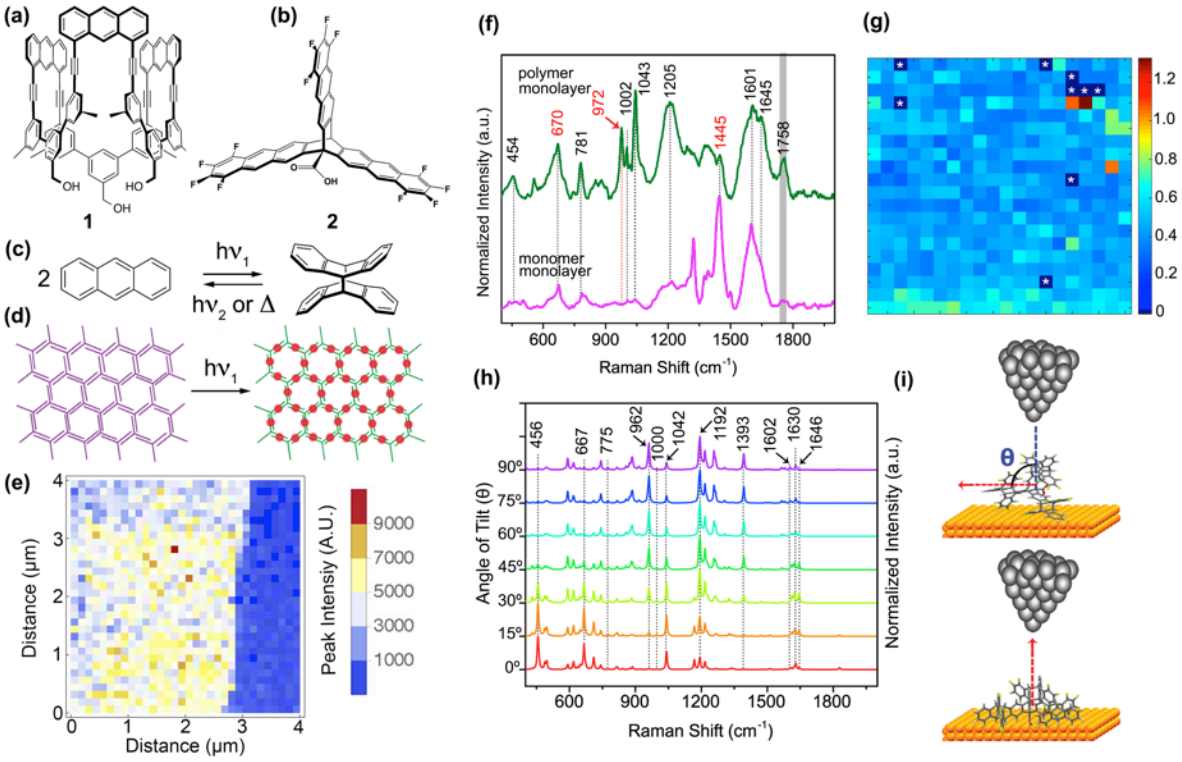

Fig. 12 Amphiphilic and shape-persistent trifunctional monomer **1** (a) and monomer **2** (b). The photochemically reactive sites (anthracene moieties) are ideally positioned at an angle of 120° with respect to each other. (c) The reaction scheme shows the reversible photochemical anthracene dimerization. (d) Packing model for the monomers in a monolayer at the air/water interface and the 2DP created from them. (e) Raman intensity image of the triple bond stretching vibration across the edge of a covalent sheet on gold. (Reprinted with permission from [236], copyright 2015 American Chemical Society). (f) Normalized average TERS spectra of monolayers of **2** and the polymer made from it deposited on Au(111). For the signal at 1758 cm^{-1} see text. (g) TERS map measured over a 100× 100 nm^2 area with a size 5×5 nm^2/pixel based on the intensity ratio of the signals at 972 and 670 cm^{-1} of a 2DP formed from **2**. For an ideal 2DP, each pixel contains of approx. 10 repeat units. Defects are indicated by dark-blue pixels with a white star. (h) Calculated TERS spectra of polymer model formed from **2** as a function of the tilt angle θ. (i) Schematics of the plane-parallel (bottom picture) and plane-perpendicular (top picture) configuration of

this model, respectively. The red and blue arrows indicate the Z direction axis of the molecule and the electromagnetic field, respectively. The molecular bending and twisting angles are held constant at 0°. (Adapted from [237], copyright 2017 Wiley-VCH Verlag GmbH)

Opilik *et al.* reported the first investigation of single/few layers of a synthetic covalent 2DP sheet by TERS imaging with a reasonably high spatial resolution (<60 nm) and a significantly improved sensitivity (contrast factor of >4000) compared to confocal Raman microscopy (Fig. 12a, e).[236] The covalent monomolecular sheets were obtained at an air/water interface by photochemically induced anthracene dimerization between the amphiphilic monomers (monomer **1**, Fig. 12c). From the TERS spectra, it was also found that the intensity of the characteristic anthracene vibrations decreased dramatically, suggesting the successful dimerization of neighboring monomer **1** based on a [4 + 4] cycloaddition, instead of [4 + 2] cycloaddition. However, the anthracene bands did not disappear completely, probably due to unreacted monomer in this film. We have recently demonstrated a 2DP formation at the air/water interface of monomer **2** with its three fluoro-substituted anthracene blades and a bridgehead carboxylic acid (Fig. 12b).[85] By irradiating monomer **2** monolayer with 365 nm laser light, direct TER spectroscopic evidence was obtained for the polymerization of the neighboring tetrafluoroanthracene units (Fig. 12 e).[237] TERS mapping revealed the polymerized films to be largely homogeneous, although defects can be seen (Fig. 12g). It was also found that polymer sheets lie flat on the Au(111) surface based on DFT calculations taking into account the surface selection rules. Statistical evaluation of the TERS data could be used to estimate a polymerization conversion of about 90 % within the covalent polymer monolayer.

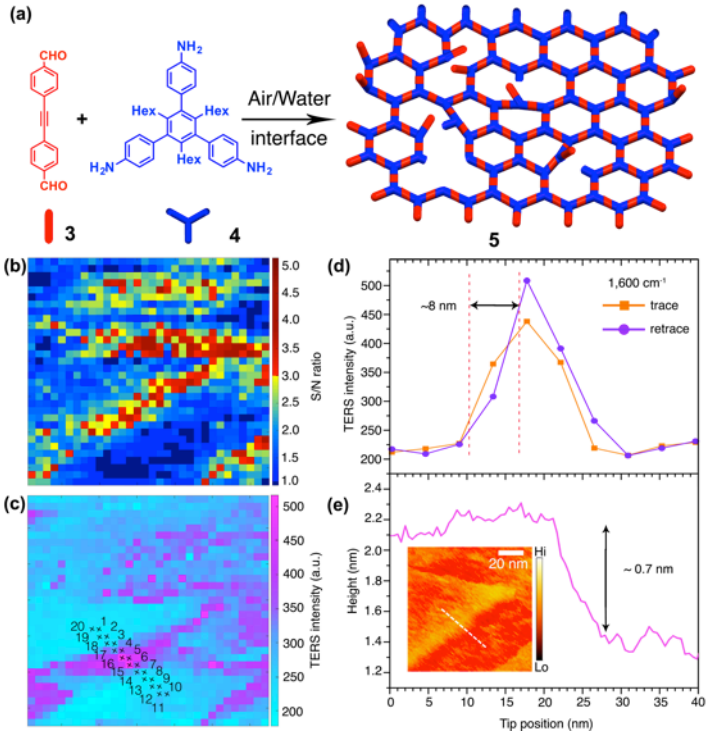

Fig. 13 (a) Synthesis of the polyimine monolayer sheet **5** with nanodefects from dialdehyde **3** and triamine **4**. (b) TERS imaging of edge-induced molecular tilt within the 2D covalent monolayer. (a) TERS signal-to-noise ratio image at 2,220 cm^{-1} and, (c) TERS intensity image at 1,600 cm^{-1} of the monolayer on a terrace of the Au(111) substrate. The maps were measured over a 100 × 100 nm^2 area with 32× 32 pixels. (d) Corresponding TERS intensity of the band at 1,600 cm^{-1} along the trace and retrace scans at the edge. The spatial resolution is estimated to be around 8 nm using a 10-90% contrast criterion. (e) STM image and corresponding topographic height profile of the terrace after TERS imaging. (Reprinted with permission from [238], copyright 2018 American Chemical Society)

We subsequently reported a 2D covalent organic monolayer synthesized from aromatic triamine and dialdehyde building blocks by dynamic imine chemistry at the air/water interface (Fig. 13a).[238] Raman/TERS-based evidence supported both the existence of imine bonds and the absence of end groups, providing strong arguments for the formation of the proposed imine-linked network in the monolayer. By introducing a triple bond into the monomer as a spectroscopic reporter, TERS imaging provided information of the chemical bonds, molecular orientation, as well as nanodefects in the resulting monolayer. Combined with DFT calculations that take into account surface selection rules, we found that the 2D covalent monolayer lies flat on the Au(111) surface, with a homogeneous orientation locked by the imine network. Approximately 3% nanodefects were observed in the networks, where the imine bonds have broken and residual segments containing the

triple bond tilt up. Additionally, using TERS imaging, we could visualize the topography and integrity of the ML sheet at Au(111) terrace steps, in which the ML smoothly covers the edge and thus will cause the orientation tilt instead of causing nanodefects or rupture. Interestingly, besides edge-induced molecular tilting, a stronger signal enhancement was observed at the terrace edges, from which a spatial resolution around 8 nm could be deduced (Fig. 13).

Conclusions and Outlook

Taking advantage of the sensitivity of SERS, the selectivity of Raman spectroscopy, the high spatial resolution of SPM, and surface selection rules, TERS has developed into a versatile tool for surface and monolayer characterization. In this review, we summarized recent works on nanoscale chemical imaging of 2D monolayers, *e.g.*, graphene, TMDCs, and 2D polymers, using TERS in a label-free and non-destructive fashion. Combined with DFT calculations that take into account the surface selection rules and dispersion interactions, TERS imaging provides structural information of such 2D monolayers in terms of nanodefects, edges, grain boundaries, local strain, end groups used, newly formed chemical bonds, molecular orientation, and intermolecular interaction at the nanoscale. Overall, TERS has matured into a powerful analytical technique at the nanoscale, and has already attracted the attention of researchers ranging from chemistry and biophysics to materials science. However, there are still several questions and challenges remaining in developing TERS into a routine and versatile technique for nanoscale chemical imaging:

Reproducible TERS tips

TERS tips play a crucial role in TERS imaging due to their impact on the enhancement effect, the spatial resolution, and signal stability. Currently, how the tip materials and morphology influence the plasmonic enhancement and the spatial resolution is still not fully understood. Under laser excitation, the morphology and plasmonic properties of the tip can be modified, resulting in the degradation of its enhancement factor and maybe also spatial resolution. Experiments with tips of different parameters (*e.g.,* materials, morphology, and coating) will provide a better understanding of what tip type is good for long-time TERS imaging and how to fabricate more robust and reproducible tips. Furthermore, for long

measurement times, Raman signals of carbonaceous decomposition products often average to two broad bands (D and G bands) centered around 1350 cm^{-1} and 1580 cm^{-1}, respectively, which has been recognized and discussed for SERS and TERS by several research groups.[165,239-241] Carbon contaminations can also lead to a distinct sharp peaks typically above 1000 cm^{-1}, which are easily misinterpreted as specific sample signals.[242] That is often a source of confusion in TERS imaging of organic materials and biological samples. How to avoid molecular photodamage and reduce production of carbonaceous contamination in the tip-sample junction during TERS imaging is another important practical problem remaining to be solved.

TERS imaging in liquids

Most TERS experiments so far have been performed under ambient or ultrahigh vacuum conditions. The liquid environment, thanks to its thermal conductivity, is expected to improve the energy dissipation under the TERS tip compared to experiments done in air. A proof-of-principle study on TERS in water was conducted in 2009 by adsorbing a self-assembled monolayer (SAM) of ethanethiolate on the Ag surface of the TERS tip to passivate it.[167] While TERS for studying electrochemical processes at liquid/solid interfaces was demonstrated independently by several groups,[141-143,243] no TERS imaging in water has been achieved so far. The key methodological problems to be solved are: (i) whether TERS tips are robust enough when operated in an aqueous environment, (ii) whether the tips have an appropriate coating to avoid current leakage in STM-TERS in liquids, and (iii) whether the tip-to-sample feedback, the enhancement, and the spatial resolution are maintained in a liquid. Performing a TERS experiment in a liquid would be extremely helpful and interesting for studying biological processes under native conditions, catalytic reactions at liquid/solid interfaces, and molecular recognition in solution with nanoscale spatial resolution.

Selection rules for TERS

In far-field Raman spectroscopy, all Raman-active modes can in principle be observed because these vibrational modes are averaged over the full space of randomly orientated molecules,[81] while in near-field TERS, the spectrum of a single molecule or monolayer will be affected by the experimental geometry (tip morphology, substrate materials, the

distance between the tip and the sample, incident and detected polarization, and the propagation direction of light).[36] Recently, Poliani *et al.* reported that the plasmon enhanced Raman signal is largely independent of the incoming light polarization in several materials, due to a modification of the Raman selection rules in TERS.[201] Moreover, the study of symmetry-imposed selection rules also facilitates the understanding of linear and nonlinear optical processes in molecules and solids.[244] However, the influence of the gap-mode on the symmetry-derived selection rules for TERS still remains to be elucidated. Several factors may break the symmetry of the molecule, including the near-field effect from the plasmon, the heating effect in the nano-cavity, and the interaction between molecules and substrates. Therefore, by taking these factors into consideration in calculations, more detailed information can be obtained from gap-mode TERS experiments.

Investigation of 2D heterostructures

2D heterostructures have been one of the most essential elements in modern semiconductor research and industry, due to revelation of unusual properties and new phenomena compared to their isolated building blocks.[245,246] Layer-by-layer stacking or lateral interfacing to combine different atomic monolayers together has opened up unprecedented opportunities to engineer 2D heteromaterials with atomic layer precision.[247] There is strong covalent bonding between the atoms within each isolated building layer, and predominantly weak van der Waals bonding between adjacent layers.[248] Due to the diffraction limit of light, existing spectroscopic methods like infrared, Raman, and photoluminescence spectroscopy that in principle could allow chemical characterization of 2D heterostructures, lack the spatial resolution necessary to analyze the heterostructures at the nanoscale. This gives rise to many open questions regarding the interlayer coupling and the nature of defects. Investigation of the van der Waals interaction within 2D heterostructures may open a new avenue for TERS application.

Acknowledgement

The authors gratefully acknowledge Dr. Guillaume Goubert for helpful discussions, ETH Zurich for financial support, and the European Research Council (ERC) for generous support

of this research via an Advanced Grant (#741431-2DNanoSpec). F.S. thanks the Chinese Scholarship Council for a Ph.D. student fellowship.

Compliance with ethical standards

Conflict of interest

The authors declare that they have no competing interests.

References

1. Butler SZ, Hollen SM, Cao L, Cui Y, Gupta JA, Gutiérrez HR, Heinz TF, Hong SS, Huang J, Ismach AF, Johnston-Halperin E, Kuno M, Plashnitsa VV, Robinson RD, Ruoff RS, Salahuddin S, Shan J, Shi L, Spencer MG, Terrones M, Windl W, Goldberger JE. Progress, Challenges, and Opportunities in Two-Dimensional Materials Beyond Graphene. ACS Nano. 2013;7 (4):2898-2926.
2. Mas-Balleste R, Gomez-Navarro C, Gomez-Herrero J, Zamora F. 2D materials: to graphene and beyond. Nanoscale. 2011;3 (1):20-30.
3. Zeng H, Cui X. An optical spectroscopic study on two-dimensional group-VI transition metal dichalcogenides. Chem Soc Rev. 2015;44 (9):2629-2642.
4. Bonaccorso F, Colombo L, Yu G, Stoller M, Tozzini V, Ferrari AC, Ruoff RS, Pellegrini V. Graphene, related two-dimensional crystals, and hybrid systems for energy conversion and storage. Science. 2015;347 (6217):1246501
5. Gao LB, Ni GX, Liu YP, Liu B, Neto AHC, Loh KP. Face-to-face transfer of wafer-scale graphene films. Nature. 2014;505 (7482):190-194.
6. Lee S-M, Kim J-H, Ahn J-H. Graphene as a flexible electronic material: mechanical limitations by defect formation and efforts to overcome. Mater Today. 2015;18 (6):336-344.
7. Suk JW, Kitt A, Magnuson CW, Hao Y, Ahmed S, An J, Swan AK, Goldberg BB, Ruoff RS. Transfer of CVD-grown monolayer graphene onto arbitrary substrates. ACS Nano. 2011;5 (9):6916-6924.
8. Liu Y, Weiss NO, Duan X, Cheng H-C, Huang Y, Duan X. Van der Waals heterostructures and devices. Nat Rev Mater. 2016;1:16042.
9. Chhowalla M, Shin HS, Eda G, Li L-J, Loh KP, Zhang H. The chemistry of two-dimensional layered transition metal dichalcogenide nanosheets. Nat Chem. 2013;5:263.
10. Schlüter AD, Payamyar P, Öttinger HC. How the World Changes By Going from One- to Two-Dimensional Polymers in Solution. Macromol Rapid Comm. 2016;37 (20):1638-1650.
11. Payamyar P, King BT, Ottinger HC, Schluter AD. Two-dimensional polymers: concepts and perspectives. Chem Commun. 2016;52 (1):18-34.

12. Dai W, Shao F, Szczerbiński J, McCaffrey R, Zenobi R, Jin Y, Schlüter AD, Zhang W. Synthesis of a Two-Dimensional Covalent Organic Monolayer through Dynamic Imine Chemistry at the Air/Water Interface. Angew Chem Int Ed. 2016;55 (1):213-217.
13. Sakamoto J, van Heijst J, Lukin O, Schlüter AD. Two-Dimensional Polymers: Just a Dream of Synthetic Chemists? Angew Chem Int Ed. 2009;48 (6):1030-1069.
14. Murray DJ, Patterson DD, Payamyar P, Bhola R, Song W, Lackinger M, Schlüter AD, King BT. Large area synthesis of a nanoporous two-dimensional polymer at the air/water interface. J Am Chem Soc. 2015;137 (10):3450-3453
15. Liu W, Luo X, Bao Y, Liu YP, Ning G-H, Abdelwahab I, Li L, Nai CT, Hu ZG, Zhao D, Liu B, Quek SY, Loh KP. A two-dimensional conjugated aromatic polymer via C–C coupling reaction. Nat Chem. 2017;9:563-570.
16. Zhao Y, Bernitzky RHM, Kory MJ, Hofer G, Hofkens J, Schlüter AD. Decorating the Edges of a 2D Polymer with a Fluorescence Label. J Am Chem Soc. 2016;138 (28):8976-8981.
17. Sahabudeen H, Qi H, Glatz BA, Tranca D, Dong R, Hou Y, Zhang T, Kuttner C, Lehnert T, Seifert G, Kaiser U, Fery A, Zheng Z, Feng X. Wafer-sized multifunctional polyimine-based two-dimensional conjugated polymers with high mechanical stiffness. Nat Commun. 2016;7:13461.
18. Boott CE, Nazemi A, Manners I. Synthetic Covalent and Non-Covalent 2D Materials. Angew Chem Int Ed. 2015;54 (47):13876-13894.
19. Ascherl L, Sick T, Margraf JT, Lapidus SH, Calik M, Hettstedt C, Karaghiosoff K, Döblinger M, Clark T, Chapman KW, Auras F, Bein T. Molecular docking sites designed for the generation of highly crystalline covalent organic frameworks. Nat Chem 2016;8 (4):310-316.
20. Love JC, Estroff LA, Kriebel JK, Nuzzo RG, Whitesides GM. Self-Assembled Monolayers of Thiolates on Metals as a Form of Nanotechnology. Chem Rev. 2005;105 (4):1103-1170.
21. van Spriel AB, van den Bogaart G, Cambi A (2015) Editorial: Membrane domains as new drug targets. Front Physiol. 2015;6 (172).
22. Gennis RB. Biomembranes: molecular structure and function. Springer Science & Business Media; 2013.
23. Wang T, Ebeling D, Yang J, Du C, Chi L, Fuchs H, Yan D. Weak Epitaxy Growth of Copper Hexadecafluorophthalocyanine (F16CuPc) on p-Sexiphenyl Monolayer Film. J Phys Chem. B 2009;113 (8):2333-2337.
24. Christian AB, Daniel JM. High-resolution atomic force microscopy and spectroscopy of native membrane proteins. Rep Prog Phys. 2011;74 (8):086601
25. Zan R, Ramasse QM, Jalil R, Bangert U. (2013) Atomic Structure of Graphene and h-BN Layers and Their Interactions with Metals. Advances in Graphene Science, Aliofkhazraei M (Ed.). InTech; 2013.
26. Huang PY, Ruiz-Vargas CS, van der Zande AM, Whitney WS, Levendorf MP, Kevek JW, Garg S, Alden JS, Hustedt CJ, Zhu Y, Park J, McEuen PL, Muller DA. Grains and grain boundaries in single-layer graphene atomic patchwork quilts. Nature. 2011;469 (7330):389-392.

27. Matei DG, Muzik H, Gölzhäuser A, Turchanin A. Structural Investigation of 1,1′ - Biphenyl-4-thiol Self-Assembled Monolayers on Au(111) by Scanning Tunneling Microscopy and Low-Energy Electron Diffraction. Langmuir. 2012;28 (39):13905-13911.

28. Mashaghi A, Mashaghi S, Reviakine I, Heeren RM, Sandoghdar V, Bonn M. Label-free characterization of biomembranes: from structure to dynamics. Chem Soc Rev. 2014;43:887-900.

29. Dietrich PM, Graf N, Gross T, Lippitz A, Krakert S, Schüpbach B, Terfort A, Unger WES. Amine species on self-assembled monolayers of ω-aminothiolates on gold as identified by XPS and NEXAFS spectroscopy. Surf Interface Anal. 2010;42 (6-7):1184-1187.

30. Kraft ML, Weber PK, Longo ML, Hutcheon ID, Boxer SG. Phase Separation of Lipid Membranes Analyzed with High-Resolution Secondary Ion Mass Spectrometry. Science. 2006;313 (5795):1948

31. Huang B, Bates M, Zhuang X. Super-resolution fluorescence microscopy. Annu Rev Biochem. 2009;78:993-1016.

32. Dazzi A, Prater CB. AFM-IR: Technology and Applications in Nanoscale Infrared Spectroscopy and Chemical Imaging. Chem Rev. 2017;117 (7):5146-5173.

33. Nowak D, Morrison W, Wickramasinghe HK, Jahng J, Potma E, Wan L, Ruiz R, Albrecht TR, Schmidt K, Frommer J, Sanders DP, Park S. Nanoscale chemical imaging by photoinduced force microscopy. Sci Adv. 2016;2 (3): e1501571.

34. de Wit G, Danial JS, Kukura P, Wallace MI. Dynamic label-free imaging of lipid nanodomains. Proc Natl Acad Sci U.S.A. 2015;112 (40):12299-12303

35. Muller EA, Pollard B, Raschke MB. Infrared Chemical Nano-Imaging: Accessing Structure, Coupling, and Dynamics on Molecular Length Scales. J Phys Chem Lett. 2015;6 (7):1275-1284.

36. Zhang R, Zhang Y, Dong Z, Jiang S, Zhang C, Chen L, Zhang L, Liao Y, Aizpurua J, Luo Y. Chemical mapping of a single molecule by plasmon-enhanced Raman scattering. Nature. 2013;498 (7452):82-86.

37. Landoulsi J, Dupres V. Direct AFM force mapping of surface nanoscale organization and protein adsorption on an aluminum substrate. Phy Chem Chem Phy. 2013;15 (21):8429-8440.

38. Beccari M, Kanjilal A, Betti MG, Mariani C, Floreano L, Cossaro A, Di Castro V. Characterization of benzenethiolate self-assembled monolayer on Cu(100) by XPS and NEXAFS. J Electron Spectrosc. 2009;172 (1):64-68.

39. Weidner T, Apte JS, Gamble LJ, Castner DG. Probing the Orientation and Conformation of α-Helix and β-Strand Model Peptides on Self-Assembled Monolayers Using Sum Frequency Generation and NEXAFS Spectroscopy. Langmuir. 2010;26 (5):3433-3440.

40. Marsi M, Casalis L, Gregoratti L, Günther S, Kolmakov A, Kovac J, Lonza D, Kiskinova M. ESCA Microscopy at ELETTRA: what it is like to perform spectromicroscopy experiments on a third generation synchrotron radiation source. J Electron Spectrosc. 1997;84 (1):73-83.

41. Bertsch PM, Hunter DB. Applications of Synchrotron-Based X-ray Microprobes. Chem Rev. 2001;101 (6):1809-1842.

42. Whitby JA, Östlund F, Horvath P, Gabureac M, Riesterer JL, Utke I, Hohl M, Sedláček L, Jiruše J, Friedli V. High spatial resolution time-of-flight secondary ion mass spectrometry for the masses: a novel orthogonal ToF FIB-SIMS instrument with in situ AFM. Adv Mater Sci Eng. 2012; 180437.

43. Ghonaim NW, Nieradko M, Xi L, Nie HY, Francis JT, Grizzi O, Yeung KKC, Lau LWM. Primary ion fluence dependence in time-of-flight SIMS of self-assembled monolayer of alkyl thiol molecules on Au(111)—Discussion of static limit. Appl Surf Sci. 2008;255 (4):1029-1032.

44. Samuel NT, Castner DG. ToF-SIMS characterization of hybridization onto self-assembled single-stranded DNA monolayers. Appl Surf Sci. 2004;231-232.

45. Kempson IM, Martin AL, Denman JA, French PW, Prestidge CA, Barnes TJ. Detecting the Presence of Denatured Human Serum Albumin in an Adsorbed Protein Monolayer Using TOF−SIMS. Langmuir. 2010;26 (14):12075-12080.

46. Frisz JF, Lou K, Klitzing HA, Hanafin WP, Lizunov V, Wilson RL, Carpenter KJ, Kim R, Hutcheon ID, Zimmerberg J. Direct chemical evidence for sphingolipid domains in the plasma membranes of fibroblasts. Proc Natl Acad Sci U.S.A. 2013;110 (8):E613-E622

47. Spengler B, Hubert M. Scanning microprobe matrix-assisted laser desorption ionization (SMALDI) mass spectrometry: instrumentation for sub-micrometer resolved LDI and MALDI surface analysis. J Am Soc Mass Spectr. 2002;13 (6):735-748.

48. Betzig E, Patterson GH, Sougrat R, Lindwasser OW, Olenych S, Bonifacino JS, Davidson MW, Lippincott-Schwartz J, Hess HF. Imaging intracellular fluorescent proteins at nanometer resolution. Science. 2006;313 (5793):1642-1645

49. Owen DM, Magenau A, Williamson DJ, Gaus K. Super-resolution imaging by localization microscopy. Methods Mol Biol. 2013;950:81-93.

50. Rust MJ, Bates M, Zhuang X. Sub-diffraction-limit imaging by stochastic optical reconstruction microscopy (STORM). Nat Meth. 2006;3 (10):793-796.

51. Heintzmann R, Jovin TM, Cremer C.2002) Saturated patterned excitation microscopy—a concept for optical resolution improvement. J Opt Soc Am A. 2002;19 (8):1599-1609.

52. Hell SW, Wichmann J. Breaking the diffraction resolution limit by stimulated emission: stimulated-emission-depletion fluorescence microscopy. Opt Lett. 1994;19 (11):780-782.

53. Donnert G, Keller J, Medda R, Andrei MA, Rizzoli SO, Lührmann R, Jahn R, Eggeling C, Hell SW. Macromolecular-scale resolution in biological fluorescence microscopy. Proc Natl Acad Sci U.S.A 2006;103 (31):11440-11445.

54. Mattheyses AL, Simon SM, Rappoport JZ. Imaging with total internal reflection fluorescence microscopy for the cell biologist. J Cell Sci. 2010;123 (21):3621.

55. Matthew RR, Michael Cai W, Xu X, John AR, SungWoo N, William PK. Measuring individual carbon nanotubes and single graphene sheets using atomic force microscope infrared spectroscopy. Nanotechnology. 2017;28 (35):355707.

56. Rajapaksa I, Uenal K, Wickramasinghe HK. Image force microscopy of molecular resonance: A microscope principle. Appl Phys Lett. 2010;97 (7):073121.

57. Andrecka J, Takagi Y, Mickolajczyk KJ, Lippert LG, Sellers JR, Hancock WO, Goldman YE, Kukura P. Interferometric Scattering Microscopy for the Study of Molecular Motors. Methods in Enzymology. Academic Press, 2016.

58. Ortega Arroyo J, Cole D, Kukura P. Interferometric scattering microscopy and its combination with single-molecule fluorescence imaging. Nat Protocols. 2016;11 (4):617-633.

59. Centrone A. Infrared Imaging and Spectroscopy Beyond the Diffraction Limit. Annu Rev Anal Chem. 2015;8 (1):101-126.

60. Chiang N, Jiang N, Chulhai DV, Pozzi EA, Hersam MC, Jensen L, Seideman T, Van Duyne RP. Molecular-Resolution Interrogation of a Porphyrin Monolayer by Ultrahigh Vacuum Tip-Enhanced Raman and Fluorescence Spectroscopy. Nano Lett. 2015;15 (6):4114-4120.

61. Höppener C, Novotny L. Antenna-Based Optical Imaging of Single Ca2+ Transmembrane Proteins in Liquids. Nano Lett. 2008;8 (2):642-646.

62. Su W, Kumar N, Mignuzzi S, Crain J, Roy D. Nanoscale mapping of excitonic processes in single-layer MoS 2 using tip-enhanced photoluminescence microscopy. Nanoscale. 2016;8 (20):10564-10569.

63. Park K-D, Khatib O, Kravtsov V, Clark G, Xu X, Raschke MB. Hybrid Tip-Enhanced Nanospectroscopy and Nanoimaging of Monolayer WSe2 with Local Strain Control. Nano Lett. 2016;16 (4):2621-2627.

64. Singh R. CV Raman and the Discovery of the Raman Effect. Physi Perspect. 2002;4 (4):399-420.

65. Smith E, Dent G. Modern Raman spectroscopy: a practical approach. John Wiley & Sons, 2013.

66. Kneipp K, Kneipp H, Itzkan I, Dasari RR, Feld MS. Ultrasensitive chemical analysis by Raman spectroscopy. Chem Rev. 1999;99 (10):2957-2976.

67. Cardinal MF, Vander Ende E, Hackler RA, McAnally MO, Stair PC, Schatz GC, Van Duyne RP. Expanding applications of SERS through versatile nanomaterials engineering. Chem Soc Rev. 2017;46 (13):3886-3903.

68. Wang Z, Zong S, Wu L, Zhu D, Cui Y. SERS-Activated Platforms for Immunoassay: Probes, Encoding Methods, and Applications. Chem Rev. 2017;117 (12):7910-7963.

69. Zrimsek AB, Chiang N, Mattei M, Zaleski S, McAnally MO, Chapman CT, Henry A-I, Schatz GC, Van Duyne RP. Single-Molecule Chemistry with Surface-and Tip-Enhanced Raman Spectroscopy. Chem Rev. 2017;117 (11):7583-7613.

70. Cialla-May D, Zheng XS, Weber K, Popp J. Recent progress in surface-enhanced Raman spectroscopy for biological and biomedical applications: from cells to clinics. Chem Soc Rev. 2017;46 (13):3945-3961.

71. Verma P. Tip-Enhanced Raman Spectroscopy: Technique and Recent Advances. Chem Rev. 2017;117 (9):6447-6466.

72. Pettinger B, Schambach P, Villagómez CJ, Scott N. Tip-Enhanced Raman Spectroscopy: Near-Fields Acting on a Few Molecules. Annu Rev Phys Chem. 2012;63 (1):379-399.

73. Pozzi EA, Goubert G, Chiang N, Jiang N, Chapman CT, McAnally MO, Henry A-I, Seideman T, Schatz GC, Hersam MC, Duyne RPV. Ultrahigh-Vacuum Tip-Enhanced Raman Spectroscopy. Chem Rev. 2017;117 (7):4961-4982.

74. Le Ru E, Etchegoin P. Principles of Surface-Enhanced Raman Spectroscopy: and related plasmonic effects. Elsevier, 2008.

75. Wessel J. (1985) Surface-enhanced optical microscopy. J Opt Soc Am B. 1985;2(9):1538-1541.

76. Stöckle RM, Suh YD, Deckert V, Zenobi R. Nanoscale chemical analysis by tip-enhanced Raman spectroscopy. Chem Phy Lett. 2000;318 (1):131-136.

77. Pettinger B, Picardi G, Schuster R, Ertl G. Surface Enhanced Raman Spectroscopy: Towards Single Moleculer Spectroscopy (E). ELECTROCHEMISTRY. 2000;68 (12):942-949.

78. Hayazawa N, Inouye Y, Sekkat Z, Kawata S. Metallized tip amplification of near-field Raman scattering. Opt Commun 2000;183 (1):333-336.

79. Anderson MS. Locally enhanced Raman spectroscopy with an atomic force microscope. Appl Phys Lett. 2000;76 (21):3130-3132.

80. Moskovits M, Suh JS. Surface selection rules for surface-enhanced Raman pectroscopy: calculations and application to the surface-enhanced Raman spectrum of phthalazine on silver. J Phy Chem. 1984; 88 (23):5526-5530.

81. Jiang S, Zhang Y, Zhang R, Hu C, Liao M, Luo Y, Yang J, Dong Z, Hou JG. Distinguishing adjacent molecules on a surface using plasmon-enhanced Raman scattering. Nat Nanotechnol. 2015;10 (10):865-869.

82. Sun M, Fang Y, Zhang Z, Xu H. Activated vibrational modes and Fermi resonance in tip-enhanced Raman spectroscopy. Phys Rev E. 2013;87 (2):020401.

83. Watanabe H, Hayazawa N, Inouye Y, Kawata S. DFT Vibrational Calculations of Rhodamine 6G Adsorbed on Silver: Analysis of Tip-Enhanced Raman Spectroscopy. J Phys Chem B. 2005;109 (11):5012-5020.

84. Jiang N, Chiang N, Madison LR, Pozzi EA, Wasielewski MR, Seideman T, Ratner MA, Hersam MC, Schatz GC, Van Duyne RP. Nanoscale Chemical Imaging of a Dynamic Molecular Phase Boundary with Ultrahigh Vacuum Tip-Enhanced Raman Spectroscopy. Nano Lett. 2016;16 (6):3898-3904.

85. Shao F, Müller V, Zhang Y, Schlüter AD, Zenobi R. Nanoscale Chemical Imaging of Interfacial Monolayers by Tip-Enhanced Raman Spectroscopy. Angew Chem Int Ed. 2017;56 (32):9361-9366.

86. Berweger S, Neacsu CC, Mao Y, Zhou H, Wong SS, Raschke MB. Optical nanocrystallography with tip-enhanced phonon Raman spectroscopy. Nat Nanotechnol. 2009;4 (8):496-499.

87. Zhang W, Yeo BS, Schmid T, Zenobi R. Single molecule tip-enhanced Raman spectroscopy with silver tips. J Phys Chem C. 2007;111 (4):1733-1738.

88. Steidtner J, Pettinger B. Tip-Enhanced Raman Spectroscopy and Microscopy on Single Dye Molecules with 15 nm Resolution. Phys Rev Lett. 2008;100 (23):236101.

89. Shi X, Coca-López N, Janik J, Hartschuh A. Advances in Tip-Enhanced Near-Field Raman Microscopy Using Nanoantennas. Chem Rev. 2017; 117 (7):4945-4960.

90. Asghari-Khiavi M, Wood BR, Hojati-Talemi P, Downes A, McNaughton D, Mechler A. Exploring the origin of tip-enhanced Raman scattering; preparation of efficient TERS probes with high yield. J Raman Spectrosc. 2012;43 (2):173-180.

91. Zhang W, Cui X, Martin OJF. Local field enhancement of an infinite conical metal tip illuminated by a focused beam. J Raman Spectrosc. 40 (10):1338-1342.

92. Hartschuh A. Tip-Enhanced Near-Field Optical Microscopy. Angew Chem Int Ed. 2009;47 (43):8178-8191.

93. Kawata S, Ichimura T, Taguchi A, Kumamoto Y. Nano-Raman Scattering Microscopy: Resolution and Enhancement. Chem Rev. 2017; 117 (7):4983-5001.

94. Taguchi A. Plasmonic tip for nano Raman microcopy: structures, materials, and enhancement. Opt Rev. 2017; 24 (3):462-469.

95. Kazemi-Zanjani N, Vedraine S, Lagugne-Labarthet F. Localized enhancement of electric field in tip-enhanced Raman spectroscopy using radially and linearly polarized light. Opt Express. 2013;21 (21):25271-25276.

96. Huang TX, Huang SC, Li MH, Zeng ZC, Wang X, Ren B. Tip-enhanced Raman spectroscopy: tip-related issues. Anal Bioanal Chem 2015;407(27):8177-8195.

97. Stadler J, Oswald B, Schmid T, Zenobi R. Characterizing unusual metal substrates for gap-mode tip-enhanced Raman spectroscopy. J Raman Spectrosc. 2013;44 (2):227-233.

98. Pettinger B, Domke KF, Zhang D, Picardi G, Schuster R. Tip-enhanced Raman scattering: Influence of the tip-surface geometry on optical resonance and enhancement. Surf Sci. 2009;603 (10):1335-1341.

99. Sattler KD. Handbook of nanophysics: nanoparticles and quantum dots. CRC press, 2016.

100. Richard-Lacroix M, Zhang Y, Dong Z, Deckert V. Mastering high resolution tip-enhanced Raman spectroscopy: towards a shift of perception. Chem Soc Rev. 2017;46 (13):3922-3944.

101. Rendell RW, Scalapino DJ. Surface plasmons confined by microstructures on tunnel junctions. Phys Rev B. 1981;24 (6):3276-3294

102. Yang Z, Aizpurua J, Xu H. Electromagnetic field enhancement in TERS configurations. J Raman Spectrosc. 2009;40 (10):1343-1348.

103. Becker SF, Esmann M, Yoo K, Gross P, Vogelgesang R, Park N, Lienau C. Gap-Plasmon-Enhanced Nanofocusing Near-Field Microscopy. ACS Photonics 2016;3(2):223-232.

104. Stadler J, Schmid T, Zenobi R. Nanoscale chemical imaging using top-illumination tip-enhanced Raman spectroscopy. Nano Lett. 2010;10 (11):4514-4520.

105. Wickramasinghe HK, Chaigneau M, Yasukuni R, Picardi G, Ossikovski R. Billion-Fold Increase in Tip-Enhanced Raman Signal. Acs Nano 2014;8 (4):3421-3426.

106. van Schrojenstein Lantman EM, Deckert-Gaudig T, Mank AJ, Deckert V, Weckhuysen BM. Catalytic processes monitored at the nanoscale with tip-enhanced Raman spectroscopy. Nat Nanotechnol. 2012;7 (9):583-586.

107. Blum C, Opilik L, Atkin JM, Braun K, Kämmer SB, Kravtsov V, Kumar N, Lemeshko S, Li JF, Luszcz K. Tip-enhanced Raman spectroscopy-an interlaboratory reproducibility and comparison study. J Raman Spectrosc. 2014;45 (1):22-31.

108. Müller V, Shao F, Baljozovic M, Moradi M, Zhang Y, Jung T, Thompson WB, King BT, Zenobi R, Schlüter AD. Structural characterization of a covalent monolayer sheet obtained by two-dimensional polymerization at an air/water interface. Angew Chem Int Ed. 2017;56(48):15262-15266.

109. Taguchi A, Hayazawa N, Furusawa K, Ishitobi H, Kawata S. Deep-UV tip-enhanced Raman scattering. J Raman Spectrosc. 2009; 40 (9):1324-1330.

110. Yang Z, Li Q, Fang Y, Sun M. Deep ultraviolet tip-enhanced Raman scattering. Chem Comm. 2011; 47 (32):9131-9133.

111. Schlegel VL, Cotton TM. Silver-island films as substrates for enhanced Raman scattering: effect of deposition rate on intensity. Anal Chem. 1991; 63 (3):241-247.

112. Golan Y, Margulis L, Rubinstein I. Vacuum-deposited gold films: I. Factors affecting the film morphology. Surf Sci. 1992;264 (3):312-326.

113. Zhang J, Matveeva E, Gryczynski I, Leonenko Z, Lakowicz JR. Metal-Enhanced Fluoroimmunoassay on a Silver Film by Vapor Deposition. J Phys Chem. B 2005;109 (16):7969-7975.

114. Huang T-X, Li C-W, Yang L-K, Zhu J-F, Yao X, Liu C, Lin K-Q, Zeng Z-C, Wu S-S, Wang X, Yang F-Z, Ren B. Rational fabrication of silver-coated AFM TERS tips with a high enhancement and long lifetime. Nanoscale 2018;10 (9):4398-4405.

115. Taguchi A, Yu J, Verma P, Kawata S. Optical antennas with multiple plasmonic nanoparticles for tip-enhanced Raman microscopy. Nanoscale. 2015; 7 (41):17424-17433.

116. Cui X, Zhang W, Yeo B-S, Zenobi R, Hafner C, Erni D. Tuning the resonance frequency of Ag-coated dielectric tips. Opt Express. 2007;15 (13):8309-8316.

117. Yeo B-S, Schmid T, Zhang W, Zenobi R. Towards rapid nanoscale chemical analysis using tip-enhanced Raman spectroscopy with Ag-coated dielectric tips. Anal BioAnal Chem. 2007;387 (8):2655-2662.

118. Yeo B-S, Zhang W, Vannier C, Zenobi R. Enhancement of Raman signals with silver-coated tips. Appl Spectros. 2006;60 (10):1142-1147

119. Zou Y, Steinvurzel P, Yang T, Crozier KB. Surface plasmon resonances of optical antenna atomic force microscope tips. Appl Phys Lett. 2009;94 (17):171107.

120. Imad M, Atsushi T, Yuika S, Satoshi K, Prabhat V. Optical antennas for tunable enhancement in tip-enhanced Raman spectroscopy imaging. Appl Phys Express. 2015;8 (3):032401.

121. Yang L-K, Huang T-X, Zeng Z-C, Li M-H, Wang X, Yang F-Z, Ren B. Rational fabrication of a gold-coated AFM TERS tip by pulsed electrodeposition. Nanoscale 2015;7 (43):18225-18231.

122. Brejna PR, Griffiths PR. Electroless deposition of silver onto silicon as a method of preparation of reproducible surface-enhanced Raman spectroscopy substrates and tip-enhanced Raman spectroscopy tips. Appl Spectros. 2010;64 (5):493-499.

123. Takayuki U, Taka-aki Y, Yuika S, Prabhat V. Fabrication of Near-Field Plasmonic Tip by Photoreduction for Strong Enhancement in Tip-Enhanced Raman Spectroscopy. Appl Phys Express. 2012;5 (5):052001.

124. Sqalli O, Bernal MP, Hoffmann P, Marquis-Weible F. Improved tip performance for scanning near-field optical microscopy by the attachment of a single gold nanoparticle. Appl Phys Lett. 2000;76 (15):2134-2136.

125. Dill TJ, Rozin MJ, Palani S, Tao AR. Colloidal Nanoantennas for Hyperspectral Chemical Mapping. ACS Nano 2016;10 (8):7523-7531.

126. Farahani JN, Pohl DW, Eisler HJ, Hecht B. Single Quantum Dot Coupled to a Scanning Optical Antenna: A Tunable Superemitter. Phys Rev Lett. 2005;95 (1):017402.

127. Weber-Bargioni A, Schwartzberg A, Cornaglia M, Ismach A, Urban JJ, Pang Y, Gordon R, Bokor J, Salmeron MB, Ogletree DF, Ashby P, Cabrini S, Schuck PJ. Hyperspectral Nanoscale Imaging on Dielectric Substrates with Coaxial Optical Antenna Scan Probes. Nano Lett. 2011;11 (3):1201-1207.

128. De Angelis F, Das G, Candeloro P, Patrini M, Galli M, Bek A, Lazzarino M, Maksymov I, Liberale C, Andreani LC, Di Fabrizio E. Nanoscale chemical mapping using three-dimensional adiabatic compression of surface plasmon polaritons. Nat Nanotechnol. 2010;5 (1):67-72.

129. Fleischer M, Weber-Bargioni A, Altoe MVP, Schwartzberg AM, Schuck PJ, Cabrini S, Kern DP. Gold Nanocone Near-Field Scanning Optical Microscopy Probes. ACS Nano 2011;5 (4):2570-2579.

130. Macpherson JV, Unwin PR. Combined Scanning Electrochemical–Atomic Force Microscopy. Anal Chem. 2000;72 (2):276-285.

131. Melmed AJ. The art and science and other aspects of making sharp tips. J Vac Sci Technol B. 1991;9 (2):601-608.

132. Stadler J, Schmid T, Zenobi R. Nanoscale Chemical Imaging Using Top-Illumination Tip-Enhanced Raman Spectroscopy. Nano Lett. 2010; 10 (11):4514-4520.

133. Sasaki SS, Perdue SM, Perez AR, Tallarida N, Majors JH, Apkarian VA, Lee J. Note: Automated electrochemical etching and polishing of silver scanning tunneling microscope tips. Rev Sci Instrum. 2013;84 (9):096109.

134. Li M, Lv R, Huang S, Dai Y, Zeng Z, Wang L, Ren B. Electrochemical fabrication of silver tips for tip-enhanced Raman spectroscopy assisted by a machine vision system. J Raman Spectrosc. 2016;47 (7):808-812.

135. Jiang N, Foley ET, Klingsporn JM, Sonntag MD, Valley NA, Dieringer JA, Seideman T, Schatz GC, Hersam MC, Van Duyne RP. Observation of Multiple Vibrational Modes in Ultrahigh Vacuum Tip-Enhanced Raman Spectroscopy Combined with Molecular-Resolution Scanning Tunneling Microscopy. Nano Lett. 2012;12 (10):5061-5067.

136. Ren B, Picardi G, Pettinger B. Preparation of gold tips suitable for tip-enhanced Raman spectroscopy and light emission by electrochemical etching. Rev Sci Instrum. 2004;75 (4):837-841.

137. Billot L, Berguiga L, De La Chapelle ML, Gilbert Y, Bachelot R. Production of gold tips for tip-enhanced near-field optical microscopy and spectroscopy: analysis of the etching parameters. Eur Phys J Appl Phys. 2005;31 (2):139-145.

138. Eligal L, Culfaz F, McCaughan V, Cade NI, Richards D. Etching gold tips suitable for tip-enhanced near-field optical microscopy. Rev Sci Instrum. 2009;80 (3):033701.

139. Kharintsev SS, Hoffmann GG, Fishman AI, Salakhov MK. Plasmonic optical antenna design for performing tip-enhanced Raman spectroscopy and microscopy. J Phys D: Appl Phys. 2013;46 (14):145501.

140. Berweger S, Atkin JM, Olmon RL, Raschke MB. Adiabatic Tip-Plasmon Focusing for Nano-Raman Spectroscopy. J Phys Chem. Lett. 2010;1 (24):3427-3432.

141. Zeng Z-C, Huang S-C, Wu D-Y, Meng L-Y, Li M-H, Huang T-X, Zhong J-H, Wang X, Yang Z-L, Ren B. Electrochemical Tip-Enhanced Raman Spectroscopy. J Am Chem Soc. 2015;137 (37):11928-11931.

142. Martín Sabanés N, Driessen LMA, Domke KF. Versatile Side-Illumination Geometry for Tip-Enhanced Raman Spectroscopy at Solid/Liquid Interfaces. Anal Chem. 2016;88 (14):7108-7114.

143. Martín Sabanés N, Ohto T, Andrienko D, Nagata Y, Domke KF. Electrochemical TERS Elucidates Potential-Induced Molecular Reorientation of Adenine/Au(111). Angew Chem Int Ed. 2017;56 (33):9796-9801.

144. Meyer R, Yao X, Deckert V. Latest instrumental developments and bioanalytical applications in tip-enhanced Raman spectroscopy. TrAC Trends in Anal Chem. 2018;102:250-258.

145. Zhang D, Wang X, Braun K, Egelhaaf H-J, Fleischer M, Hennemann L, Hintz H, Stanciu C, Brabec CJ, Kern DP, Meixner AJ. Parabolic mirror-assisted tip-enhanced spectroscopic imaging for non-transparent materials. J Raman Spectrosc. 2009;40 (10):1371-1376.

146. Neacsu CC, Dreyer J, Behr N, Raschke MB. Scanning-probe Raman spectroscopy with single-molecule sensitivity. Phys Rev B. 2006;73 (19):193406.

147. Hartschuh A, Sánchez EJ, Xie XS, Novotny L. High-Resolution Near-Field Raman Microscopy of Single-Walled Carbon Nanotubes. Phys Rev Lett. 2003;90 (9):095503.

148. Wang J, Wu X, Wang R, Zhang M. Detection of Carbon Nanotubes Using Tip-Enhanced Raman Spectroscopy. In: Electronic Properties of Carbon Nanotubes. InTech, 2011.

149. Kalkbrenner T, Ramstein M, Mlynek J, Sandoghdar V. A single gold particle as a probe for apertureless scanning near-field optical microscopy. J Microsc. 2001;202 (1):72-76.

150. Christiane H, Lukas N. Imaging of membrane proteins using antenna-based optical microscopy. Nanotechnology. 2008;19 (38):384012.

151. Le Nader V, Mevellec J-Y, Minea T, Louarn G. Gold Nanoparticles as Probes for Nano-Raman Spectroscopy: Preliminary Experimental Results and Modeling . Inter J Opt. 2012; 591083.

152. Stadler J, Schmid T, Opilik L, Kuhn P, Dittrich PS, Zenobi R. Tip-enhanced Raman spectroscopic imaging of patterned thiol monolayers. Beilstein J Nanotechnol. 2011;2:509.

153. Opilik L, Dogan Ü, Szczerbiński J, Zenobi R. Degradation of silver near-field optical probes and its electrochemical reversal. Appl Phys Lett. 2015;107 (9):091109.

154. Barrios CA, Malkovskiy AV, Kisliuk AM, Sokolov AP, Foster MD Highly Stable, Protected Plasmonic Nanostructures for Tip Enhanced Raman Spectroscopy. J Phys Chem C. 2009;113 (19):8158-8161.

155. Pieczonka NPW, Aroca RF. Inherent Complexities of Trace Detection by Surface-Enhanced Raman Scattering. ChemPhysChem. 2005;6 (12):2473-2484.

156. Waterhouse GIN, Bowmaker GA, Metson JB. Oxygen chemisorption on an electrolytic silver catalyst: a combined TPD and Raman spectroscopic study. Applied Surf Sci. 2003;214 (1):36-51.

157. Martina I, Wiesinger R, Schreiner M. Micro-Raman investigations of early stage silver corrosion products occurring in sulfur containing atmospheres. J Raman Spectrosc. 2013;44 (5):770-775.

158. Yeo B-S, Schmid T, Zhang W, Zenobi R. A Strategy to Prevent Signal Losses, Analyte Decomposition, and Fluctuating Carbon Contamination Bands in Surface-Enhanced Raman Spectroscopy. Appl Spectros. 2008;62 (6):708-713.

159. Agapov RL, Sokolov AP, Foster MD. Protecting TERS probes from degradation: extending mechanical and chemical stability. J Raman Spectrosc. 2013;44 (5):710-716.

160. Yeo B-S, Stadler J, Schmid T, Zenobi R, Zhang W. Tip-enhanced Raman Spectroscopy - Its status, challenges and future directions. Chem Phys Lett. 2009;472 (1-3):1-13.

161. Stadler J, Schmid T, Zenobi R. Developments in and practical guidelines for tip-enhanced Raman spectroscopy. Nanoscale. 2012 4 (6):1856-1870.

162. Zhang W, Schmid T, Yeo B-S, Zenobi R. Near-field heating, annealing, and signal loss in tip-enhanced Raman spectroscopy. J Phys Chem C. 2008;112 (6):2104-2108.

163. Schmid T, Opilik L, Blum C, Zenobi R. Nanoscale Chemical Imaging Using Tip-Enhanced Raman Spectroscopy: A Critical Review. Angew Chem Int Ed. 2013;52 (23):5940-5954.

164. Domke KF, Zhang D, Pettinger B. Enhanced Raman Spectroscopy: Single Molecules or Carbon? J Phys Chem C. 2007;111 (24):8611-8616.

165. Chaigneau M, Picardi G, Ossikovski R. Tip enhanced Raman spectroscopy evidence for amorphous carbon contamination on gold surfaces. Surf Sci. 2010;604 (7):701-705.

166. Opilik L, Dogan Uz, Li C-Y, Stephanidis B, Li J-F, Zenobi R. Chemical Production of Thin Protective Coatings on Optical Nanotips for Tip-Enhanced Raman Spectroscopy. J Phys Chem C. 2016;120 (37):20828-20832

167. Schmid T, Yeo B-S, Leong G, Stadler J, Zenobi R. Performing tip-enhanced Raman spectroscopy in liquids. J Raman Spectrosc. 2009;40 (10):1392-1399.

168. Kumar N, Spencer SJ, Imbraguglio D, Rossi AM, Wain AJ, Weckhuysen BM, Roy D. Extending the plasmonic lifetime of tip-enhanced Raman spectroscopy probes. Phys Chem Chem Phys 2016;18 (19):13710-13716.

169. Paulite M, Blum C, Schmid T, Opilik L, Eyer K, Walker GC, Zenobi R. Full Spectroscopic Tip-Enhanced Raman Imaging of Single Nanotapes Formed from β-Amyloid(1–40) Peptide Fragments. Acs Nano 2013;7 (2):911-920.

170. Liao M, Jiang S, Hu C, Zhang R, Kuang Y, Zhu J, Zhang Y, Dong Z. Tip-Enhanced Raman Spectroscopic Imaging of Individual Carbon Nanotubes with Subnanometer Resolution. Nano Lett. 2016;16 (7):4040-4046.

171. Lin WI, Shao F, Stephanidis B, Zenobi R. Tip-enhanced Raman spectroscopic imaging shows segregation within binary self-assembled thiol monolayers at ambient conditions. Anal Bioanal Chem. 2015;407 (27):8197-8204.

172. Opilik L, Bauer T, Schmid T, Stadler J, Zenobi R. Nanoscale chemical imaging of segregated lipid domains using tip-enhanced Raman spectroscopy. Phys Chem Chem Phys. 201113 (21):9978-9981.

173. Ichimura T, Watanabe H, Morita Y, Verma P, Kawata S, Inouye Y. Temporal Fluctuation of Tip-Enhanced Raman Spectra of Adenine Molecules. J Phys Chem C. 2007;111 (26):9460-9464.

174. Abbe E. Beiträge zur Theorie des Mikroskops und der mikroskopischen Wahrnehmung. Archiv für mikroskopische Anatomie 1873;9 (1):413-418.

175. Rayleigh L. XII. On the manufacture and theory of diffraction-gratings. The London, Edinburgh, and Dublin Philosophical Magazine and Journal of Science. 1874;47 (310):81-93

176. Zhang R, Zhang X, Wang H, Zhang Y, Jiang S, Hu C, Zhang Y, Luo Y, Dong Z. Distinguishing Individual DNA Bases in a Network by Non-Resonant Tip-Enhanced Raman Scattering. Angew Chem Int Ed. 2017;56 (20):5561-5564.

177. Chiang N, Chen X, Goubert G, Chulhai DV, Chen X, Pozzi EA, Jiang N, Hersam MC, Seideman T, Jensen L, Van Duyne RP. Conformational Contrast of Surface-Mediated Molecular Switches Yields Ångstrom-Scale Spatial Resolution in Ultrahigh Vacuum Tip-Enhanced Raman Spectroscopy. Nano Lett. 2016;16 (12):7774-7778.

178. Tallarida N, Lee J, Apkarian VA. Tip-Enhanced Raman Spectromicroscopy on the Angstrom Scale: Bare and CO-Terminated Ag Tips. ACS Nano. 2017;11 (11):11393-11401.

179. Lee J, Tallarida N, Chen X, Liu P, Jensen L, Apkarian VA. Tip-Enhanced Raman Spectromicroscopy of Co(II)-Tetraphenylporphyrin on Au(111): Toward the Chemists' Microscope. ACS Nano. 2017;11 (11):11466-11474.

180. Lin X-M, Deckert-Gaudig T, Singh P, Siegmann M, Kupfer S, Zhang Z, Gräfe S, Deckert V. Direct base-to-base transitions in ssDNA revealed by tip-enhanced Raman Scattering. arXiv preprint. 2016; arXiv:160406598.

181. Deckert-Gaudig T, Kurouski D, Hedegaard MA, Singh P, Lednev IK, Deckert V. Spatially resolved spectroscopic differentiation of hydrophilic and hydrophobic domains on individual insulin amyloid fibrils. Sci. Rep. 2016;6:33575.

182. Uzunbajakava N, Lenferink A, Kraan Y, Volokhina E, Vrensen G, Greve J, Otto C. Nonresonant Confocal Raman Imaging of DNA and Protein Distribution in Apoptotic Cells. Biophys J. 2003;84 (6):3968-3981.

183. Bonhommeau S, Lecomte S. Tip-Enhanced Raman Spectroscopy: A Tool for Nanoscale Chemical and Structural Characterization of Biomolecules. ChemPhysChem. 2017;19 (1):8-18.

184. Klingsporn JM, Jiang N, Pozzi EA, Sonntag MD, Chulhai D, Seideman T, Jensen L, Hersam MC, Duyne RPV. Intramolecular Insight into Adsorbate–Substrate Interactions via Low-Temperature, Ultrahigh-Vacuum Tip-Enhanced Raman Spectroscopy. J Am Chem Soc. 2014;136 (10):3881-3887.

185. Trautmann S, Aizpurua J, Gotz I, Undisz A, Dellith J, Schneidewind H, Rettenmayr M, Deckert V. A classical description of subnanometer resolution by atomic features in metallic structures. Nanoscale. 2017;9 (1):391-401.

186. Benz F, Schmidt MK, Dreismann A, Chikkaraddy R, Zhang Y, Demetriadou A, Carnegie C, Ohadi H, de Nijs B, Esteban R, Aizpurua J, Baumberg JJ (2016) Single-molecule optomechanics in "picocavities". Science. 2016;354 (6313):726-729.

187. Meng L, Yang Z, Chen J, Sun M. Effect of electric field gradient on sub-nanometer spatial resolution of tip-enhanced Raman spectroscopy. Sci Rep. 2015;5:9240.

188. Duan S, Tian G, Ji Y, Shao J, Dong Z, Luo Y. Theoretical Modeling of Plasmon-Enhanced Raman Images of a Single Molecule with Subnanometer Resolution. J Am Chem Soc. 2015;137 (30):9515-9518.

189. Duan S, Tian G, Luo Y. Theory for Modeling of High Resolution Resonant and Nonresonant Raman Images. J Chem Theory Comput. 2016;12 (10):4986-4995.

190. Zhang C, Chen B-Q, Li Z-Y (2015) Optical Origin of Subnanometer Resolution in Tip-Enhanced Raman Mapping. J Phys Chem. C 119 (21):11858-11871.

191. Roelli P, Galland C, Piro N, Kippenberg TJ. Molecular cavity optomechanics as a theory of plasmon-enhanced Raman scattering. Nat Nanotechnol. 2015;11:164-169.

192. Latorre F, Kupfer S, Bocklitz T, Kinzel D, Trautmann S, Grafe S, Deckert V. Spatial resolution of tip-enhanced Raman spectroscopy - DFT assessment of the chemical effect. Nanoscale 2016;8 (19):10229-10239.

193. Liu P, Chulhai DV, Jensen L (2017) Single-Molecule Imaging Using Atomistic Near-Field Tip-Enhanced Raman Spectroscopy. ACS Nano 2017;11 (5):5094-5102.

194. Sheppard N, Erkelens J. Vibrational Spectra of Species Adsorbed on Surfaces: Forms of Vibrations and Selection Rules for Regular Arrays of Adsorbed Species. Appl Spectros. 1984;38 (4):471-485.

195. Moskovits M. Surface selection rules. J Chem Phys. 1982;77 (9):4408-4416.

196. Madey TE, Yates Jr JT. Vibrational spectroscopy of molecules on surfaces. Springer Science & Business Media, 2013.

197. Creighton JA. Surface raman electromagnetic enhancement factors for molecules at the surface of small isolated metal spheres: The determination of adsorbate orientation from sers relative intensities. Surf Sci. 1983;124 (1):209-219.

198. Landau LD, Bell J, Kearsley M, Pitaevskii L, Lifshitz E, Sykes J. Electrodynamics of Continuous Media. Eelsevier, 2013.

199. Tsuboi M, Benevides JM, Thomas Jr GJ. Raman Tensors and their application in structural studies of biological systems. Proc Jpn Acad B. 2009;85 (3):83-97.

200. Tsuboi M, Thomas GJ. Raman Scattering Tensors in Biological Molecules and Their Assemblies. Appl Spectrosc Rev. 1997;32 (3):263-299.

201. Poliani E, Wagner MR, Vierck A, Herziger F, Nenstiel C, Gannott F, Schweiger M, Fritze S, Dadgar A, Zaumseil J, Krost A, Hoffmann A, Maultzsch J. Breakdown of Far-Field Raman Selection Rules by Light–Plasmon Coupling Demonstrated by Tip-Enhanced Raman Scattering. J Phys Chem Lett. 2017;8 (22):5462-5471.

202. Novoselov KS, Geim AK, Morozov SV, Jiang D, Zhang Y, Dubonos SV, Grigorieva IV, Firsov AA. Electric field effect in atomically thin carbon films. Science. 2004;306 (5696):666-669.

203. Beams R. Tip-enhanced Raman scattering of graphene. J Raman Spectrosc. 2017;49 (1):157-167.

204. Wu J-B, Lin M-L, Cong X, Liu H-N, Tan P-H. Raman spectroscopy of graphene-based materials and its applications in related devices. Chem Soc Rev. 2018;47 (5):1822-1873.

205. Beams R. Tip-enhanced Raman scattering of graphene. J Raman Spectrosc. 2018;49 (1):157-167.

206. Zandiatashbar A, Lee G-H, An SJ, Lee S, Mathew N, Terrones M, Hayashi T, Picu CR, Hone J, Koratkar N. Effect of defects on the intrinsic strength and stiffness of graphene. Nat Commun. 2014;5:3186.

207. Hwangbo Y, Lee C-K, Kim S-M, Kim J-H, Kim K-S, Jang B, Lee H-J, Lee S-K, Kim S-S, Ahn J-H. Fracture characteristics of monolayer CVD-graphene. Sci Rep. 2014;4:4439.

208. Schwierz F. Graphene transistors. Nat Nanotechnol. 2010;5 (7):487-496.

209. Yazyev OV, Helm L. Defect-induced magnetism in graphene. Phys Rev B. 2007;75 (12):125408.

210. Wei Y, Wu J, Yin H, Shi X, Yang R, Dresselhaus M. The nature of strength enhancement and weakening by pentagon–heptagon defects in graphene. Nat Mater. 2012;11 (9):759-763.

211. Banhart F, Kotakoski J, Krasheninnikov AV. Structural Defects in Graphene. ACS Nano. 2011;5 (1):26-41.

212. Stadler J, Schmid T, Zenobi R. Nanoscale Chemical Imaging of Single-Layer Graphene. Acs Nano. 2011;5 (10):8442-8448.

213. Mignuzzi S, Kumar N, Brennan B, Gilmore IS, Richards D, Pollard AJ, Roy D. Probing individual point defects in graphene via near-field Raman scattering. Nanoscale. 2015;7 (46):19413-19418.

214. Su W, Kumar N, Dai N, Roy D. Nanoscale mapping of intrinsic defects in single-layer graphene using tip-enhanced Raman spectroscopy. Chem Commun. 2016;52 (53):8227-8230.

215. Li X, Liu Y, Zeng Z, Wang P, Fang Y, Zhang L. Investigation on tip enhanced Raman spectra of graphene. Spectrochim Acta A Mol Biomol Spectrosc. 2018;190:378-382.

216. Su W, Roy D. Visualizing graphene edges using tip-enhanced Raman spectroscopy. J Vac Sci Technol B Nanotechnol Microelectron. 2013;31 (4):041808.

217. Beams R, Cançado LG, Oh S-H, Jorio A, Novotny L. Spatial Coherence in Near-Field Raman Scattering. Phys Rev Lett. 2014;113 (18):186101

218. Beams R, Cançado LG, Novotny L. Low Temperature Raman Study of the Electron Coherence Length near Graphene Edges. Nano Lett. 2011;11 (3):1177-1181.

219. Park KD, Raschke Markus B, Atkin Joanna M, Lee Young H, Jeong Mun S. Probing Bilayer Grain Boundaries in Large-Area Graphene with Tip-Enhanced Raman Spectroscopy. Adv Mater. 2017;29 (7):1603601.

220. Snitka V, Rodrigues RD, Lendraitis V. Novel gold cantilever for nano-Raman spectroscopy of graphene. Microelectron Eng. 2011;88 (8):2759-2762.

221. Ryan B, Luiz Gustavo C, Ado J, Vamivakas AN, Lukas N. Tip-enhanced Raman mapping of local strain in graphene. Nanotechnology 2015;26 (17):175702.

222. Geim AK, Grigorieva IV. Van der Waals heterostructures. Nature. 2013;499 (7459):419-425.

223. Chow PK, Jacobs-Gedrim RB, Gao J, Lu T-M, Yu B, Terrones H, Koratkar N. Defect-Induced Photoluminescence in Monolayer Semiconducting Transition Metal Dichalcogenides. ACS Nano. 2015;9 (2):1520-1527.

224. Bao W, Borys NJ, Ko C, Suh J, Fan W, Thron A, Zhang Y, Buyanin A, Zhang J, Cabrini S, Ashby PD, Weber-Bargioni A, Tongay S, Aloni S, Ogletree DF, Wu J, Salmeron MB, Schuck PJ. Visualizing nanoscale excitonic relaxation properties of disordered edges and grain boundaries in monolayer molybdenum disulfide. Nat Commun. 2015.6:7993.

225. Su W, Kumar N, Mignuzzi S, Crain J, Roy D. Nanoscale mapping of excitonic processes in single-layer MoS2 using tip-enhanced photoluminescence microscopy. Nanoscale 2016;8 (20):10564-10569.

226. Rahaman M, Rodriguez RD, Plechinger G, Moras S, Schüller C, Korn T, Zahn DRT. Highly Localized Strain in a MoS2/Au Heterostructure Revealed by Tip-Enhanced Raman Spectroscopy. Nano Lett. 2017;17 (10):6027-6033.

227. Milekhin AG, Rahaman M, Rodyakina EE, Latyshev AV, Dzhagan VM, Zahn DRT. Giant gap-plasmon tip-enhanced Raman scattering of MoS2 monolayers on Au nanocluster arrays. Nanoscale. 2018;10 (6):2755-2763.

228. Kory MJ, Wörle M, Weber T, Payamyar P, van de PollStan W, Dshemuchadse J, Trapp N, Schlüter AD. Gram-scale synthesis of two-dimensional polymer crystals and their structure analysis by X-ray diffraction. Nat Chem. 2014;6 (9):779-784.

229. Kissel P, Murray DJ, Wulftange WJ, Catalano VJ, King BT. A nanoporous two-dimensional polymer by single-crystal-to-single-crystal photopolymerization. Nat Chem. 2014;6 (9):774-778.

230. Kissel P, Erni R, Schweizer WB, Rossell MD, King BT, Bauer T, Götzinger S, Schlüter AD, Sakamoto J. A two-dimensional polymer prepared by organic synthesis. Nat Chem. 20124 (4):287-291.

231. Bhola R, Payamyar P, Murray DJ, Kumar B, Teator AJ, Schmidt MU, Hammer SM, Saha A, Sakamoto J, Schlüter AD, King BT. A Two-Dimensional Polymer from the Anthracene Dimer and Triptycene Motifs. J Am Chem Soc. 2013;135 (38):14134-14141.

232. Payamyar P, Kaja K, Ruiz-Vargas C, Stemmer A, Murray DJ, Johnson CJ, King BT, Schiffmann F, VandeVondele J, Renn A, Götzinger S, Ceroni P, Schütz A, Lee L-T, Zheng Z, Sakamoto J, Schlüter AD. Synthesis of a Covalent Monolayer Sheet by Photochemical Anthracene Dimerization at the Air/Water Interface and its Mechanical Characterization by AFM Indentation. Adv Mater. 2014;26 (13):2052-2058.

233. Bauer T, Zheng Z, Renn A, Enning R, Stemmer A, Sakamoto J, Schlüter AD. Synthesis of Free-Standing, Monolayered Organometallic Sheets at the Air/Water Interface. Angew Chem Int Ed. 2011;50 (34):7879-7884.

234. Dong R, Pfeffermann M, Liang H, Zheng Z, Zhu X, Zhang J, Feng X. Large-Area, Free-Standing, Two-Dimensional Supramolecular Polymer Single-Layer Sheets for Highly Efficient Electrocatalytic Hydrogen Evolution. Angew Chem Int Ed. 2015;54 (41):12058-12063.

235. Sakamoto R, Hoshiko K, Liu Q, Yagi T, Nagayama T, Kusaka S, Tsuchiya M, Kitagawa Y, Wong W-Y, Nishihara H. A photofunctional bottom-up bis(dipyrrinato)zinc(II) complex nanosheet. Nat Commun. 2016;6:6713.

236. Opilik L, Payamyar P, Szczerbiński J, Schütz AP, Servalli M, Hungerland T, Schlüter AD, Zenobi R. Minimally Invasive Characterization of Covalent Monolayer Sheets Using Tip-Enhanced Raman Spectroscopy. ACS Nano 2015;9 (4):4252-4259.

237. Müller V, Shao F, Baljozovic M, Moradi M, Zhang Y, Jung T, Thompson WB, King BT, Zenobi R, Schlüter AD. Structural Characterization of a Covalent Monolayer Sheet Obtained by Two-Dimensional Polymerization at an Air/Water Interface. Angew Chem Int Ed. 2017;56 (48):15262-15266.

238. Shao F, Dai W, Zhang Y, Zhang W, Schlüter AD, Zenobi R. Chemical Mapping of Nanodefects within 2D Covalent Monolayers by Tip-Enhanced Raman Spectroscopy. ACS Nano. 2018;12 (5):5021-5029.

239. Richards D, Milner RG, Huang F, Festy F Tip-enhanced Raman microscopy: practicalities and limitations. J Raman Spectrosc. 2003;34 (9):663-667.

240. Bjerneld EJ, Svedberg F, Johansson P, Käll M. Direct Observation of Heterogeneous Photochemistry on Aggregated Ag Nanocrystals Using Raman Spectroscopy: The Case of Photoinduced Degradation of Aromatic Amino Acids. J Phys Chem A. 2004;108 (19):4187-4193.

241. Matikainen A, Nuutinen T, Itkonen T, Heinilehto S, Puustinen J, Hiltunen J, Lappalainen J, Karioja P, Vahimaa P. Atmospheric oxidation and carbon contamination of silver and its effect on surface-enhanced Raman spectroscopy (SERS). Sci Rep. 2016;6:37192.

242. Schmid T, Opilik L, Blum C, Zenobi R. Nanoscale Chemical Imaging Using Tip-Enhanced Raman Spectroscopy: A Critical Review. Angew Chem Int Ed. 2013;52 (23):5940-5954.

243. Kurouski D, Mattei M, Van Duyne RP. Probing Redox Reactions at the Nanoscale with Electrochemical Tip-Enhanced Raman Spectroscopy. Nano Lett. 2015;15 (12):7956-7962.

244. Jorio A, Mueller NS, Reich S. Symmetry-derived selection rules for plasmon-enhanced Raman scattering. Phys Rev B 2017;95 (15):155409.

245. Geim A, Grigorieva I. Van der Waals heterostructures. Nature 2013;499 (7459):419-425

246. Georgiou T, Jalil R, Belle BD, Britnell L, Gorbachev RV, Morozov SV, Kim Y-J, Gholinia A, Haigh SJ, Makarovsky O, Eaves L, Ponomarenko LA, Geim AK, Novoselov KS, Mishchenko A. Vertical field-effect transistor based on graphene-WS2 heterostructures for flexible and transparent electronics. Nat Nanotechnol. 20123;8 (2):100-103.

247. Gong Y, Lin J, Wang X, Shi G, Lei S, Lin Z, Zou X, Ye G, Vajtai R, Yakobson BI, Terrones H, Terrones M, Tay Beng K, Lou J, Pantelides ST, Liu Z, Zhou W, Ajayan PM. Vertical and in-plane heterostructures from WS2/MoS2 monolayers. Nat Mater. 2014;13 (12):1135-1142.

248. Britnell L, Ribeiro RM, Eckmann A, Jalil R, Belle BD, Mishchenko A, Kim Y-J, Gorbachev RV, Georgiou T, Morozov SV, Grigorenko AN, Geim AK, Casiraghi C, Neto AHC, Novoselov KS. Strong Light-Matter Interactions in Heterostructures of Atomically Thin Films. Science. 2013;340 (6138):1311-1314.